Measurement report: Formation and brownness of aqueous secondary organic aerosol from the aged biomass-burning emissions in the Sichuan Basin, China

Chao Peng[1,2,3,4], Yan Ding[4], Zhenliang Li[1,2,3], Tianyu Zhai[4], Xinping Yang[4], Mi Tian[6], Yang Chen[5], Xin Long[5], Haohui Tang[6], Guangming Shi[7], Liuyi Zhang[8], Kangyin Zhang[8], Fumo Yang[7], and Chongzhi Zhai[1,2,3]

[1]Chongqing Academy of Ecology and Environmental Sciences, Chongqing, 401336, China

[2]Chongqing Branch Academy of Chinese Research Academy of Environmental Sciences, Chongqing, 401336, China

[3]Chongqing Key Laboratory of Urban Atmospheric Environment Observation and Pollution Prevention, Chongqing, 401336, China

[4]Chinese Research Academy of Environmental Sciences, Beijing 100012, China

[5]Chongqing Institute of Green and Intelligent Technology, Chinese Academy of Sciences, Chongqing, 400714, China

[6]College of Environment and Ecology, Chongqing University, Chongqing, 400045, China

[7]College of Carbon Neutrality Future Technology, Sichuan University, Chengdu, 610065, China

[8]Chongqing Three Gorges University, Wanzhou, 404000, China

Correspondence: Chao Peng (pengchao0623@sina.com) and Chongzhi Zhai (czz66818@sina.com)

Abstract. Secondary organic aerosol (SOA), formed via complex chemical mechanisms, is the major contributor to atmospheric aerosol pollution and climate forcing worldwide. Aqueous-phase oxidation serve as an important pathway for SOA formation, with aqueous SOA (aqSOA) exhibiting light absorption across the ultraviolet to visible range. Here, we reported the formation and absorption properties of aqSOA in the Sichuan Basin, China. The results show that aqSOA mainly originated from aged biomass-burning emissions via aqueous-phase reactions rather than from photochemical reactions, particularly under high aerosol liquid water content (ALWC) conditions during the polluted period. Substantial enhancement of brown carbon (BrC) absorption by SOA was observed between 370 nm and 660 nm (27.5%−43.2%). These findings highlighted the significant contribution of aqSOA formation from aged biomass-burning emissions to the BrC budget and absorption, especially at night. The mean aerosol absorption Ångström exponents between 370 nm and 880 nm (AAE$_{370-880}$) was 1.95, higher than values reported for fresh and photochemically aged biomass-burning emissions. This study elucidates the formation and light-absorbing characteristics of aqSOA derived from aged biomass-burning emissions and highlights the important role of aqueous-phase reactions in aerosol pollution and radiative absorption.

Keywords: Particulate matter; Secondary organic aerosol; Aqueous-phase oxidation; Aged biomass-burning emissions; Brown carbon.

1 Introduction

Organic aerosol (OA) constitutes a dominant fraction (20 to 90%) of atmospheric aerosol, with significant implications for air quality and climate forcing (Jimenez et al., 2009). Field observations consistently indicate that secondary OA (SOA), formed by atmospheric oxidation of volatile organic compounds (VOCs) and primary OA (POA), accounts for most OA worldwide (Ervens et al., 2011; Huang et al., 2014; Kourtchev et al., 2016). Recent results demonstrate that aqueous-phase oxidation serves as an important pathway for SOA formation and these SOA products (aqSOA) exhibit light absorption across the ultraviolet (UV) to visible (Vis) range (Gilardoni et al., 2016; Lim et al., 2010; McNeill 2015; Powelson et al., 2014; Sun et al., 2010). However, the formation mechanisms and absorption properties of aqSOA remain poorly understood, which hinders efforts to improve air quality and reduce uncertainties in global climate estimates.

An increasing number of studies suggest that aqSOA represents a major component of SOA formed in fogs, clouds, and aerosol water (Ervens et al., 2011; Ortiz-Montalvo et al., 2012; Tan et al., 2012; Xu et al., 2022). Oxygenated VOCs (OVOCs) with high water solubility and low Henry's law constants (i.e., methylglyoxal and glycolaldehyde) are important aqSOA precursors (Ortiz-Montalvo et al., 2012; Tan et al., 2012). A few laboratory studies have also shown that levoglucosan and phenolic species produced from biomass burning could also act as aqSOA precursors (Yu et al., 2016; Zhao et al., 2014). Gilardoni et al. (2016) reported direct ambient observations of aqSOA formation from biomass-burning emissions in fog water and wet aerosol. Additionally, recent studies indicate that aqSOA with high molecular weight (i.e., 4-ethylphenol) formed by aqueous-phase photochemical oxidation can exhibit strong light absorptivity within the UV range (Herrmann et al., 2015; Ye et al., 2019). Previous laboratory studies also demonstrate that certain aqSOA conponents, such as π-conjugated compounds and imidazole with C=N bonds produced by aldol condensation and aqueous-phase carbonyl compound reactions respectively, would strongly absorb light at the near-UV region (Drozd and McNeill,

3

2014; Kampf et al., 2012; Nozière and Esteve, 2007; Powelson et al., 2014). Despite numerous studies on the formation and optical properties of aqSOA, limited ambient observations still hinder a better understanding of its role in atmospheric chemistry and climate.

China has experienced severe $PM_{2.5}$ pollution under stagnant high-humidity conditions, during which SOA, a major $PM_{2.5}$ component, originated largely from fossil fuel combustion and biomass burning (Huang et al., 2014; Wang et al., 2016; Wang et al., 2021; Xu et al., 2022). Field observations indicate that highly oxidized SOA could form through aqueous-phase processing driven by acid-catalyzed oxidation (Meng et al., 2020; Xu et al., 2017), and aqSOA derives from biomass-burning OA (BBOA) and fossil-fuel OA via aqueous-phase reactions (Wang et al., 2021; Zhao et al., 2019). A few laboratory studies have found that aqueous-phase reactions serve as an important oxidation pathway for nitrophenol products (i.e., 5-nitrovanillin and 4-nitroguaiacol) with exhibit strong UV absorption and higher formation/transformation rates in more acidic solutions (Kroflic et al., 2015; Li et al., 2023; Pang et al., 2019; Yang et al., 2021). However, observations of aqSOA formation and optical properties in China remain limited, with most research focusing on the North China Plain (NCP). Similar to the NCP, the Sichuan Basin (SCB) characterized by high humidity and frequent biomass burning is also the main region with severe aerosol pollution in China (Tian et al., 2019; Wang et al., 2018; Yang et al., 2011).

Previous research has indicated that aqSOA from different regions can exhibit distinct formation mechanisms and optical properties due to varying emission sources and ambient conditions (Bao et al., 2023; Bao et al., 2024; Wang et al., 2021; Xu et al., 2017). For instance, Wang et al. (2021) revealed fast aqueous-phase conversion of fossil-fuel primary organic aerosol (FF-POA) to aqSOA under high-humidity conditions during a winter haze event in Beijing, noting that the resulting aqSOA exhibited much lower light absorption than its primary precursor due to decreased aromaticity. Similarly, Huang et al. (2023) illustrated that the aqueous-phase oxidation of fossil fuel combustion emissions played a critical role in SOA formation under high

4

删除[Mi]: reported

删除[Mi]: research on its

删除[Mi]: to

删除[Mi]: the

删除[Mi]: of aqSOA

删除[Mi]: the

删除[Mi]: when

删除[Mi]: as

删除[Mi]: the

删除[Mi]: was

删除[Mi]: d

删除[Mi]: is formed

删除[Mi]: were

删除[Mi]: with

删除[Mi]: and

删除[Mi]: were observed

删除[Mi]: on

删除[Mi]: are

删除[Mi]: and

删除[Mi]: concentrate

删除[Mi]: ed

删除[Mi]: ,

删除[Mi]: the diverse

删除[Mi]: winter haze event

删除[Mi]: and found

RH conditions during winter. Xu et al. (2022) indicated that biomass burning serves as a significant non-fossil source of aqSOA under high RH and high aerosol liquid water content (ALWC) conditions, especially during fall-to-winter period when open burning of post-harvest agricultural crop residues is widespread in China. While aqSOA formation has been extensively studied during winter, autumn—despite featuring both high ALWC and strong biomass burning emissions—has received considerably less attention (Feng et al., 2022; Qiu et al., 2016; Zhao et al., 2019). In contrast to these studies in NCP, research in the SCB has shown that the effect of aqueous-phase reactions on oxygenated OA (OOA) formation was significant when ALWC was below 200 μg m^{-3}, but became insignificant at ALWC > 200 μg m^{-3}. Additionally, aqueous-phase oxidation probably did not contribute to the decay of BrC during summer in the SCB (Bao et al., 2024). It should be pointed out that autumn is the typical biomass burning season following the harvest of rape and rice in the SCB, and the contribution of biomass burning to OA is significantly higher in autumn than in other seasons (Chen et al., 2017; Tao et al., 2014; Yang et al., 2019). In summary, the intensive biomass burning emissions and high ALWC during autumn in the SCB likely result in aqSOA formation pathways that differ from those in other seasons. To date, few studies have explored the dynamic evolution and optical properties of aqSOA in the SCB, especially during autumn, leaving ambient aqSOA processing poorly understood. Therefore, a more detailed characterization of aqSOA formation and optical properties is of great importance to reveal the key factors contributing to haze formation in this region.

Here, a time-of-flight aerosol chemical speciation monitor (ToF-ACSM) and a series of collocated instruments were deployed to characterize the dynamic evolution of aqSOA from biomass burning under real ambient conditions. The study was conducted in a typical city with relatively serious air pollution in SCB from October 21 to November 23, 2022. Observations revealed that haze formation was largely driven by BBOA and aqSOA. We demonstrated that aqSOA originated from aged BBOA via aqueous-phase reactions. Furthermore, results showed that aqSOA derived from aged BBOA exhibited strong UV absorption and contributed to positive

5

129 radiative forcing. These results elucidate the formation and brownness of aqSOA from

130 aged biomass-burning emissions, providing insights for better simulating its impacts

131 on atmospheric chemistry and climate.

2 Methods

2.1 Sampling site

134 An intensive field campaign investigating the chemical and physical properties

135 of aerosols was conducted at a site in Yongchuan (29°21′25″ N, 105°54′6″ E), a city

136 experiencing severe aerosol pollution from October 21 to November 23, 2022. This

137 site is representative of an urban environment, surrounded by restaurants, shopping

138 malls, and residential buildings, and is located in a parallel ridge-and-valley area

139 between the two megacities in SCB (Chongqing center and Chengdu) (Fig. S1). It is

140 primarily influenced by multiple local emission sources, including traffic (arterial

141 roads to the east 600 m and west 300 m) and a variety of residential activities (i.e.,

142 biomass burning and fossil fuel combustion). The absence of dynamic interference

143 from neighboring buildings allowed the measurements to clearly capture the

144 characteristics and evolution of haze pollution at this location.

2.2 Instrumentation

146 During the campaign, the non-refractory aerosol (NR-PM$_{2.5}$) species, including

147 OA, ammonium (NH$_4$), nitrates (NO$_3$), sulfates (SO$_4$), and chlorides (Chl), were

148 measured on-line by ToF-ACSM (Aerodyne Research Inc.). Ambient aerosols were

149 pumped into ToF-ACSM at a flow rate of 3 L min^{-1} through a PM$_{2.5}$ cyclone

150 (URG-2000-30ED) and a Nafion dryer (MD-110-48S, Perma Pure, Inc.) reducing the

151 relative humidity to below 30%. The measurement principle was described in detail in

152 the previous studies (Fröhlich et al., 2013; Ng et al., 2011c).

153 A seven-wavelength Aethalometer (AE33, Magee Scientific) was used to

154 measure the aerosol light absorption (Abs$_\lambda$) and equivalent black carbon (BC$_\lambda$) mass

155 concentrations in real time at 370, 470, 520, 590, 660, 880, and 950 nm. The sampled

particles were dried by a Nafion dryer (MD-70024S-3, Perma Pure, Inc.) before entering into AE33. The light attenuation coefficients were converted to Abs_λ based on the real-time compensation parameter, and the nonlinear loading effects of quartz filters were dealt with on-line by the parallel measurements of attenuation values (ATN1 and ATN2) (Coen et al., 2010; Drinovec et al., 2015). The scattering effects of quartz filters were modified automatically by a fixed multiple scattering parameter (2.14). Detailed measurement methods and principles of AE33 can be found in Drinovec et al. (2015).

During the campaign, the gaseous species (including O_3, NO_2, and CO) were continuously measured by gas analyzers (49i, 42i, and 48i, Thermo Scientific), that were maintained and calibrated weekly. Hourly meteorological parameters data including temperature (T), relative humidity (RH) and $PM_{2.5}$ mass concentrations were obtained on-line from the measurements at the National Environmental Monitoring Station, which was close to our sampling site (http://www.cnemc.cn/).

2.3 Data analysis

2.3.1 ToF-ACSM data analysis

The raw mass spectra data measured by ToF-ACSM were analyzed using Tofware v2.5.13 (Tofwerk AG) in Igor Pro 6.37 (WaveMetrics, Inc.). The ionization efficiency (IE) and relative ionization efficiency (RIEs) were regularly calibrated using a scanning mobility particle sizer with a differential mobility analyzer (SMPS 3081A, TSI) and a condensation particle counter (CPC 3775, TSI). The comprehensive overview of the operation and calibration procedures of ToF-ACSM can be found in Bao et al. (2023). In accordance with previous studies, the default RIEs values for OA, NO_3, and Chl were set to 1.4, 1.1, and 1.3, respectively (Canagaratna et al., 2007; Elser et al., 2016). The IE value (236 ions pg^{-1}) and RIEs of SO_4 (1.2) and NH_4 (4.3) were estimated from the calibrations of pure ammonium nitrate and ammonium sulfate, respectively. Meanwhile, a particle collection efficiency (CE) was introduced to compensate for the particle loss, as the acidity, the

contribution of ammonium nitrate (ANMF) and phase state changed the particle bounce effects at the vaporizer (Matthew et al., 2008). Middlebrook et al. (2012) developed a CE algorithm for ToF-ACSM to quantify the aerosol species. Their results indicated that a constant CE value of 0.45 should be used when: (1) the ANMF is below 40%, or (2) particles are partially or fully neutralized. In this study, aerosol particles were dried by Nafion dryer (RH < 30%) before sampling by ToF-ACSM, and the ANMF was always below 40%. As shown in Fig. S2, the average ratio of the measured NH_4 to the predicted NH_4 needed to fully neutralize the SO_4, NO_3 and Chl was approximately 1. All of these conditions did not affect the CE value that had usually been used at this site. The typical default CE value (0.5) was applied during the whole sampling period, which was consistent with previous research (Bao et al., 2025; Peng et al., 2025; Sun et al., 2016a; Sun et al., 2016b; Zhao et al., 2019). While the typical default CE is 10% higher than 0.45, the difference is small considering the 30% uncertainty determined for CE (Bahreini et al., 2009). Additionally, the strong correlation between NR-PM$_{2.5}$ and PM$_{2.5}$ mass concentrations supported that the CE value was reasonable (Fig. S3).

The mass spectral matrix of OA for m/z 10−120 was analyzed by positive matrix factorization (PMF) and multilinear engine (ME2) implemented via SoFi (Source Finder) (version 6.3, Canonaco et al., 2013; Paatero 1999; Paatero and Tapper 1994). Briefly, an unconstrained PMF analysis was performed to determine the number and types of source factors. Then, the constrained ME2 approach was applied to minimize rotational ambiguity by testing a-values from 0 to 1 with a step of 0.1 (Elser et al., 2016; Wang et al., 2019b; Zhong et al., 2021). Ions with a signal-to-noise ratio (S/N) lower than 0.2 were discarded, while those with S/N between 0.2−2 were downweighted by a factor of 2 (Bao et al., 2023; Paatero and Hopke 2003). Finally, five OA factors were resolved with the rotational parameter set to zero ($f_{peak} = 0$), including three POA factors (i.e., BBOA, coal-combustion OA (CCOA), and hydrocarbon-like OA (HOA)) and two SOA factors (i.e., OOA and aqSOA) (Fig. S9 and S10). We present detailed diagnostic plots of the PMF results in the supporting information (Fig. S4−S10), and the details of OA source apportionment procedures

8

删除[Mi]: vaporiser

删除[Mi]:

删除[Mi]: with

删除[Mi]: the

删除[Mi]: used

删除[Mi]: s

删除[Mi]: ,

删除[Mi]: t

删除[Mi]: restriction

删除[Mi]: method

删除[Mi]: used

删除[Mi]: PMF

删除[Mi]: the

删除[Mi]: The i

删除[Mi]: data

删除[Mi]: and

删除[Mi]: from

删除[Mi]: function of

删除[Mi]: were identified

删除[Mi]: . The

are described in SI Text S1.

2.3.2 Aerosol liquid water content

ALWC is controlled by meteorological conditions (T and RH) as well as by inorganic and organic components. During the campaign, ALWC controlled by inorganic fraction was estimated by the ISORROPIA-II thermodynamic model, based on mass concentrations of ammonium, nitrates, sulfates, and chlorides measured by ToF-ACSM, together with the meteorological parameters (T and RH) from National Environmental Monitoring Station (Fountoukis and Nenes, 2007). The calculations were performed in forward type and metastable mode within ISORROPIA-II (Hennigan et al., 2015). The model simulated the thermodynamic equilibrium of the $NH_4^+-SO_4^{2-}-NO_3^--Cl^--H_2O$ system and subsequently calculated ALWC. Following established methods, the organic contribution to ALWC was estimated using the Zdanovskii−Stokes−Robinson (ZSR) mixing rule as discussed in SI Text S2 (Guo et al., 2015; Huang et al., 2020; Nguyen et al., 2016; Xu et al., 2022). In this study, the ALWC with organic species ranged from 0.1 to 35.2 µg m^{-3}, with an average of 1.9 ± 3.0 µg m^{-3}, taking up 3.7 ± 2.2% of total ALWC. As organic species had minor effects on total ALWC (< 5%), the ALWC was determined only considering inorganic species (Chen et al., 2021; Guo et al., 2015; Liu et al., 2017).

2.3.3 Light absorption measurements

The Abs$_\lambda$ was partitioned into contributions from BC and brown carbon (BrC, a group of colored OA compounds) (Abs$_{\lambda,BC}$ and Abs$_{\lambda,BrC}$) (Abs$_\lambda$=Abs$_{\lambda,BC}$+Abs$_{\lambda,BrC}$) and characterized by the absorption Ångström exponents (AAE) (Laskin et al., 2015). Here, Abs$_\lambda$ was derived from BC$_\lambda$ mass concentrations at each wavelength using the mass absorption cross-section (MAC$_\lambda$) (Abs$_\lambda$=BC$_\lambda$×MAC$_\lambda$), with MAC$_\lambda$ values assumed as 18.47, 14.54, 13.14, 11.58, 10.35, 7.77, and 7.19 m^2 g^{-1} at 370, 470, 520, 590, 660, 880, and 950 nm, respectively (Drinovec et al., 2015; Zhu et al., 2017). Absorbance at 880 nm (Abs$_{880}$) was attributed solely to BC, then the following

formula was used to determine $Abs_{\lambda,BC}$ values: $Abs_{\lambda,BC}=Abs_{880}\times(880/\lambda)^{-AAE_{BC}}$ (Drinovec et al., 2015; Kirchstetter and Novakov, 2004; Moosmüller et al., 2009; Qin et al., 2018; Zhu et al., 2017). The AAE of BC (AAE_{BC}) was obtained from the equality: $AAE_{BC}=-\log_{10}(Abs_{880}/Abs_{950})\div\log_{10}(880/950)$ (Wang et al., 2021). A detailed description of $Abs_{\lambda,BC}$ and $Abs_{\lambda,BrC}$ calculations is provided in SI Text S3. Previous studies have demonstrated that AAE_{BC} is sensitive to the refractive index, size distribution, and coating state of carbonaceous aerosols (Gyawali et al., 2009; Lack and Langridge, 2013; Li et al., 2019). In this study, the uncertainties in Abs_{BC} and Abs_{BrC} estimations were analyzed (Text S3). The relative uncertainty ranges of Abs_{BC} and Abs_{BrC} were [−46%, +21%] and [−112%, +42%] at 370 nm, respectively. $Abs_{\lambda,BrC}$ comprises contributions from primary and secondary BrC ($Abs_{\lambda,BrC,pri}$ and $Abs_{\lambda,BrC,sec}$). $Abs_{\lambda,BrC,sec}$ was calculated by a minimum R-squared (MRS) method at each wavelength (Wang et al., 2019b; Wu and Yu, 2016; Wu et al., 2024). Further details on the MRS method and $Abs_{\lambda,BrC,sec}$ estimation are provided in SI Text S3.

The light absorption contribution of different OA components at each wavelength as analyzed using multiple linear regression (MLR), expressed as: $Abs_{BrC}=a\times[OOA]+b\times[BBOA]+c\times[CCOA]+d\times[aqSOA]+e\times[HOA]$ (Qin et al., 2018; Xie et al., 2019). Here, [OOA], [BBOA], [CCOA], [aqSOA], and [HOA] denote the mass concentrations of the corresponding OA components. The coefficients a–e are constants, used to optimize the Abs_{λ} of each OA component, and equivalent to MAC values at each wavelength (i.e., a–e at 370 nm represented $MAC_{370,OOA}$, $MAC_{370,BBOA}$, $MAC_{370,CCOA}$, $MAC_{370,aqSOA}$, and $MAC_{370,HOA}$, respectively). Here, the normalized mean bias (NMB), root mean square error (RMSE), and index of agreement (IOA) were used to evaluate the performance of the MLR method (SI Text S4) (Li et al., 2011). The IOA values for $Abs_{370,BrC}$ and $Abs_{470,BrC}$ (0.99 and 1.00) exceeded 0.95. The slopes of the linear regression between the AE33-measured and MLR-estimated absorption coefficients were 0.81 and 0.96 for $Abs_{370,BrC}$ and $Abs_{470,BrC}$ (close to unity), respectively. These results indicate good agreement between AE33 measurement and the MLR-reconstructed $Abs_{370,BrC}$.

3 Results and discussion

3.1 Enhanced OA formation from BBOA and aqSOA during pollution periods

The temporal variations of $PM_{2.5}$ species concentrations, meteorological parameters, $Abs_{370,BrC}$ and $MAC_{370,BrC}$ during the campaign are shown in Fig. 1. Wind speeds were consistently low (0.3 ± 0.2 m s^{-1}), indicating stagnant atmospheric conditions throughout the study period. The total $PM_{2.5}$ (BC+NR-$PM_{2.5}$) mass concentrations ranged from 7.0 to 175.5 μg m^{-3}, with an average of 48.4 ± 27.8 μg m^{-3}. The average concentrations of OA, NO_3, SO_4, NH_4, Chl, and BC were 24.1 ± 18.1, 8.3 ± 6.2, 6.2 ± 3.4, 5.2 ± 2.7, 0.2 ± 0.1, and 4.7 ± 2.9 μg m^{-3}, accounting for 46.6 ± 10.7%, 17.7 ± 8.0%, 13.2 ± 4.4%, 11.2 ± 2.7%, 0.3 ± 0.2%, and 10.1 ± 5.5% of total $PM_{2.5}$, respectively. OA constituted the largest fraction of $PM_{2.5}$, highlighting its importance in $PM_{2.5}$ pollution in the SCB (Bao et al., 2023; Wang et al., 2018). The OA fractions of $PM_{2.5}$ in this study are as high as those reported in wintertime studies in the SCB, and significantly higher than those observed in winter in other regions of China (Table S1). Meanwhile, elevated levels of $Abs_{370,BrC}$ and $MAC_{370,BrC}$, ranging from 5.8 to 210.2 Mm^{-1} (42.4 ± 28.5 Mm^{-1}) and from 0.6 to 7.0 m^2 g^{-1} (2.1 ± 0.9 m^2 g^{-1}) respectively, were observed during the campaign.

According to the Chinese National Ambient Air Quality Standard (NAAQS) (GB 3095-2012) (MEP, 2012), the Grade I and Grade II 24-hour limits for $PM_{2.5}$ are 35 μg m^{-3} and 75 μg m^{-3}, respectively. The Grade II limit, based on WHO Phase-1 interim target (IT-1), is higher than the WHO Air Quality Guideline (AQG) value (15 μg m^{-3}), the EU daily limit (25 μg m^{-3}), and U.S. 24-hour standard (35 μg m^{-3}). During the campaign, the average of $PM_{2.5}$ concentration was 1.4 times of the Grade I limit (35 μg m^{-3}). Pollution periods (PP) were defined as days with daily $PM_{2.5}$ mass concentrations exceeding the Grade II limit (75 μg m^{-3}), while days with $PM_{2.5}$ below 75 μg m^{-3} were classified as clean periods (CP). During PP, the average mass concentrations of BC+NR-$PM_{2.5}$ and OA were 102.3 ± 26.9 and 57.4 ± 22.5 μg m^{-3}, 2.5 and 3.1 times of those during CP, respectively. As shown in Fig. 2, the chemical

11

composition of $PM_{2.5}$ differed substantially between PP and CP. Compared with other species, a significantly higher contribution of OA was observed during PP (56.6%) than CP (46.6%) (Student's t-test, $p < 0.001$) (Fig. 2).

Here, five OA factors were resolved by PMF model with detailed information provided in SI Text S1, and the mass spectra of these factors are shown in Fig. S9. HOA was characterized by alkyl fragment ion series at $C_nH^+_{2n-1}$ and $C_nH^+_{2n+1}$ (i.e., m/z 41, 43, 55, and 57), typical of primary combustion emissions (Elser et al., 2016; Lanz et al., 2007). BBOA was identified by prominent signals at m/z 60 (mainly $C_2H_4O_2^+$) and m/z 73 (mainly $C_3H_5O_2^+$), which are fragments of levoglucosan and mannosan from incomplete biomass burning (Alfarra et al., 2007). CCOA showed high signals of unsaturated hydrocarbon ion fragments such as PAH-related ion fragments (i.e., m/z 77, 91, 115), indicative of traditional coal combustion (Sun et al., 2016a). OOA was distinguished by a dominant signal at m/z 44 (mainly CO_2^+) and strong correlation with oxygenated ions (Ng et al., 2011b). aqSOA also correlated strongly with oxygenated ions (i.e, m/z 43 (mainly $C_2H_3O^+$) and m/z 44), and exhibited a notably higher signal at m/z 29 (mainly CHO^+) compared with other OA factors, consistent with previous reports (Sun et al., 2016a; Xu et al., 2019; Zhao et al., 2019; Zhong et al., 2021). Moreover, BBOA showed significant correlations with m/z 60 (mainly $C_2H_4O_2^+$) and m/z 73 (Pearson's r^2 (r^2) = 0.85, 0.80, $p < 0.001$); CCOA was strongly correlated with Chl and m/z 115 (r^2 = 0.56, 0.48, $p < 0.001$); HOA was correlated with NO_2 and m/z 41 (r^2 = 0.47, 0.59, $p < 0.001$); OOA and aqSOA were significantly correlated with NO_3/NH_4 (r^2 = 0.77, 0.75, $p < 0.001$) and SO_4/ALWC (r^2 = 0.67, 0.85, $p < 0.001$), respectively (Fig. S10). These results confirm the robustness and physicochemical plausibility of the five OA factors identified in this study. Overall, the average concentration of BBOA was 8.6 ± 7.7 μg m^{-3} and accounted for the highest proportion of OA ($34.8 \pm 11.2\%$), followed by OOA (5.5 ± 3.5 μg m^{-3}, $21.7 \pm 11.4\%$), CCOA (4.0 ± 3.3 μg m^{-3}, $15.7 \pm 7.1\%$), HOA (3.5 ± 2.8 μg m^{-3}, $14.6 \pm 8.1\%$), and aqSOA (3.3 ± 2.9 μg m^{-3}, $13.2 \pm 5.9\%$) (Fig. 1). These results demonstrated BBOA as the dominant component of OA in autumn in the SCB. It is worth noting that fractions of BBOA to OA in this study were much higher than those

328 reported in wintertime studies in China (Table S1).

329 It should be noted that the contributions of BBOA and aqSOA to OA increased
330 from CP (31.7% and 12.6%) to PP (38.6% and 14.1%), while the contributions of
331 CCOA, HOA, and OOA decreased. Significantly higher RH and ALWC were
332 observed during PP (58.5 ± 12.4% and 69.4 ± 30.3 μg m^{-3}) than CP (49.8 ± 8.9% and
333 37.1 ± 20.8 μg m^{-3}) ($p < 0.001$), whereas temperature showed no significant
334 difference ($p > 0.1$). The average wind speed was 0.32 ± 0.18 m s^{-1} during CP, 1.3
335 times that during PP. These results indicated that the atmosphere during PP was
336 characterized by stagnation, higher RH, and elevated ALWC, which likely led to the
337 distinct sources and chemical processing of OA compared with CP.

338 Compared with CP, OA concentration exhibited an obvious diurnal variation
339 during PP. As shown in Fig. 2, the OA concentration peaked was observed at 12:00
340 local time (LT) (82.7 μg m^{-3}) during daytime in PP, while in CP the peak occurred at
341 21:00 LT. During PP, OA concentration increased rapidly at a rate of 7.8 μg m^{-3} hr^{-1}
342 from 09:00 to 12:00 LT, accompanied by a significant decrease in NO$_3$. BBOA and
343 aqSOA concentrations showed similar diurnal patterns to OA, with high values during
344 daytime and a rapidly increased from 09:00 to 12:00 LT during PP. Previous studies
345 have indicated that aqSOA mass spectrum showed a higher signal at m/z 29 (CHO$^+$)
346 than other OA factors (Gilardoni et al., 2016; Meng et al., 2020; Wang et al., 2021).
347 During PP, the tracer ion fragments for BBOA (m/z 60) and aqSOA (m/z 29), peaked
348 at 12:00 LT (1.2 μg m^{-3}) and 13:00 LT (4.3 μg m^{-3}), respectively. Additionally,
349 ALWC correlated more strongly with aqSOA concentration ($r^2 = 0.86$, $p < 0.001$) than
350 with BBOA concentration ($r^2 = 0.58$, $p < 0.001$). Both ALWC and aqSOA
351 concentration peaked at 13:00 LT, later than BBOA peak (12:00 LT), supporting that
352 ALWC might play a significant role in the chemical processing that converts BBOA
353 to aqSOA during PP. In contrast, odd oxygen (O$_x$ = O$_3$ + NO$_2$) showed weak
354 correlations with both OOA and aqSOA concentrations throughout the campaign ($p >$
355 0.1, data not shown). Although the average O$_x$ concentration was higher during PP
356 (51.1 ± 19.6 ppb) than CP (36.9 ± 14.0 ppb), no significant correlation was observed
357 in either period. These results suggested that photochemical reactions might play a

13

删除[Chao]:
删除[Mi]: contributions
删除[Mi]: Additionally, s
删除[Mi]: but not
删除[Mi]: in a stagnant state with
删除[Mi]: relatively
删除[Mi]: during PP
删除[Mi]: might
删除[Mi]: a
删除[Mi]: largely different
删除[Mi]: during
删除[Mi]: and PP
删除[Mi]: the
删除[Mi]: of OA concentration was exhibited
删除[Mi]: (82.7 μg m^{-3})
删除[Mi]: in the
删除[Mi]: during
删除[Mi]: observed
删除[Mi]: at night during CP
删除[Mi]: Moreover
删除[Mi]: rapidly
删除[Mi]: with
删除[Mi]: of
删除[Mi]: during PP
删除[Mi]: Meanwhile,
删除[Mi]: concentration
删除[Mi]: in the
删除[Mi]: research
删除[Mi]: peaks of m/z 60 and m/z 29 concentrations,
删除[Mi]: of
删除[Mi]: were observed
删除[Mi]: the correlation between
删除[Mi]: and
删除[Mi]: s

limited role in SOA formation in this study.

In summary, these results suggested that OA was the dominant component of PM$_{2.5}$, especially during PP in the SCB. During PP, BBOA and aqSOA contributed significantly to the daytime increasing in OA concentration. Previous studies have shown that autumn harvest period − specifically October and November − is characterized by intensified biomass burning in the SCB, primarily due to post-harvest crop-residue burning (Chen et al., 2017; Tao et al., 2014). Thus, daytime aqSOA formation during PP might be related to high aerosol water content and BBOA emissions (Bao et al., 2023; Chen et al., 2017; Chen et al., 2019; Tao et al., 2014). Additionally, Gilardoni et al. (2016) also found that aqSOA such as guaiacol dimer (C$_{14}$H$_{14}$O$_4^+$) could be formed from aged biomass-burning emissions in both fog water and wet aerosol, especially under high ALWC conditions. To further explore the formation of aqSOA from biomass-burning emissions via aqueous-phase reactions, the next section will discuss the dynamic evolution of aqSOA in relation to BBOA.
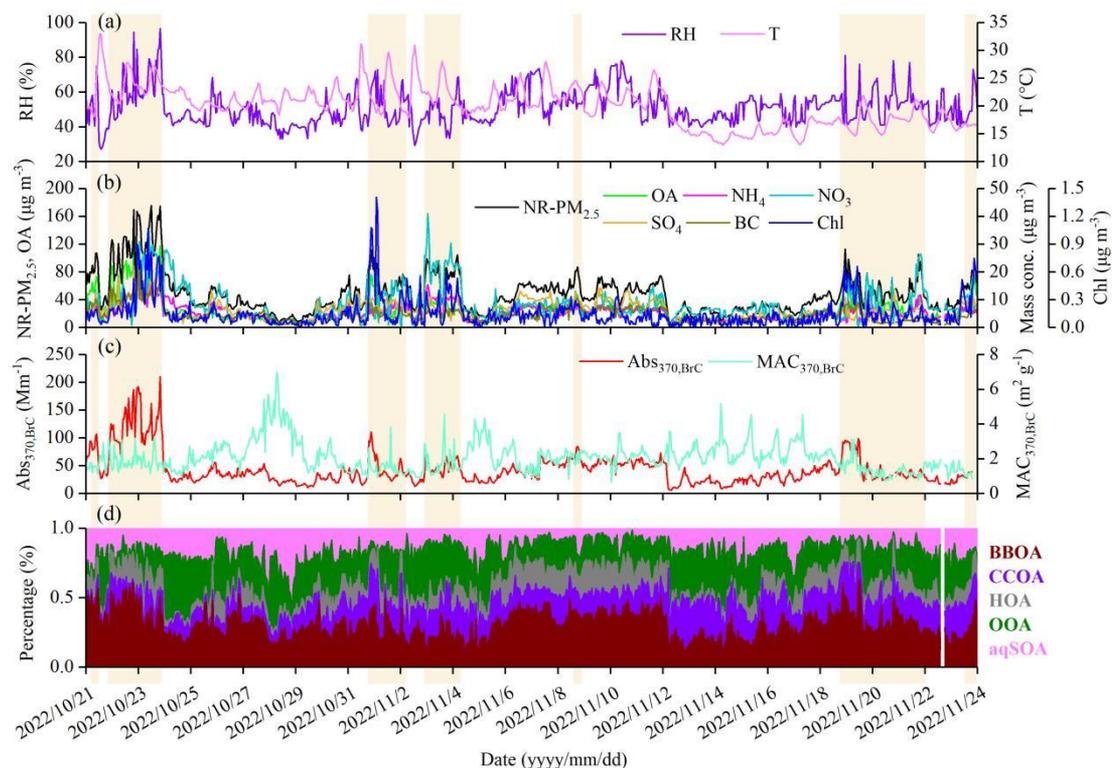
Figure 1. Time series of **(a)** RH and T, **(b)** NR-PM$_{2.5}$ species measured by ToF-ACSM and BC, **(c)** Abs$_{370,BrC}$ and MAC$_{370,BrC}$, and **(d)** mass fraction of OA factors during the campaign. The pollution period (BC+NR-PM$_{2.5}$ > 75 µg m^{-3}) is highlighted by the shaded areas.

14

376
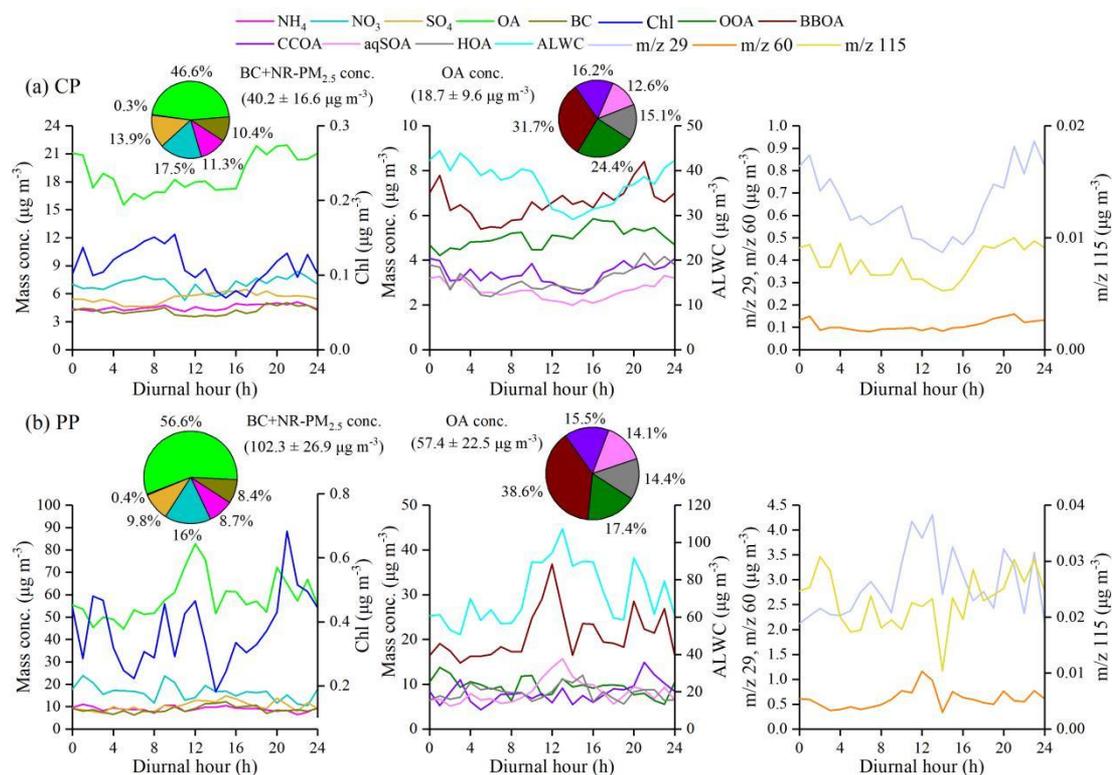
Figure 2. Diurnal variations of PM$_{2.5}$ species, BC, OA factors, m/z 29, m/z 60, and m/z 115 mass

concentrations during **(a)** clean period (CP) (BC+NR-PM$_{2.5}$ < 75 µg m^{-3}) and **(b)** polluted period

(PP) (BC+NR-PM$_{2.5}$ > 75 µg m^{-3}). The pie charts in the left side of **(a)** and **(b)** show the average

mass contributions of different chemical compositions to BC+NR-PM$_{2.5}$ during CP and PP,

respectively. Meanwhile, the average mass contributions of OOA, BBOA, CCOA, aqSOA, and

HOA in OA are shown in the pie charts in the middle of **(a)** and **(b)**, respectively.

3.2 Biomass-burning emissions as precursors for aqSOA

Figure 3 shows a strong positive correlation between the mass fraction (%) of

aqSOA in total PM$_{2.5}$ and ALWC during the campaign ($r^2 = 0.64$, $p < 0.001$). The

contribution of aqSOA increased with increasing f_{29} values (the normalized signal at

m/z 29). It was important to note that the aqSOA factor showed significantly higher

f_{29} and f_{60} values (0.167 and 0.011) than the OOA factor (0.017 and 0.002) (Fig. S9).

Moreover, both aqSOA concentrations and f_{29} were strongly correlated with ALWC

($r^2 = 0.85, 0.73$, $p < 0.001$) (Fig. 3). The average oxygen-to-carbon ratio (O:C) ratio of

aqSOA factor (0.85) was 2.7 times that of BBOA factor (0.31), whereas the

hydrogen-to-carbon (H:C) ratios were similar (1.74 for aqSOA and 1.81 for BBOA,

15

删除[Mi]: .

删除[Mi]: the

删除[Mi]: the

删除[Mi]: e of

删除[Mi]:   mass spectrum

删除[Mi]:   (normalized mass spectrum signal at m/z 60)

删除[Mi]:   , respectively

删除[Mi]:   well

删除[Mi]:   During the campaign, t

删除[Mi]:   value of the

删除[Mi]:   (0.31)

删除[Mi]:   . However

删除[Mi]:   similar

删除[Mi]:   ratio

删除[Mi]:   values of aqSOA factor and BBOA factor were observed

respectively), indicating replacement of a hydrogen atom by a OH moiety (Lim et al., 2010; Ng et al., 2011a). These results were similar to aqSOA observed in Italy and Beijing (Gilardoni et al., 2016; Zhao et al., 2019).

Previous studies indicated that aqueous-phase processes could play a role in SOA formation from fossil fuel emissions (Ervens et al., 2011; Huang et al., 2023; Wang et al., 2021; Xu et al., 2022; Yan et al., 2017). For example, Wang et al. (2021) and Xu et al. (2022) have highlighted the role of aqueous-phase reactions in SOA formation, particularly in regions with substantial anthropogenic emissions. In this study, a strong anticorrelation was observed between the mass fraction of fossil-fuel related OA components (sum of CCOA, HOA and OOA) and ALWC at high f_{29} values ($r^2 =$ 0.48, $p < 0.001$, data not shown), consistent with recent findings (Wang et al., 2021). This indicated that aqSOA might also be produced by aqueous-phase reactions of fossil-fuel related OA components.

Figure 4 shows the relationships between ALWC and the concentrations of OA factors as well as f_{29} during the campaign. The mass concentrations of all five resolved OA factors generally increased with rising ALWC. However, compared with other OA factors, aqSOA and BBOA increased more significantly, from 1.1 and 4.9 $\mu g\ m^{-3}$ to 5.2 and 10.8 $\mu g\ m^{-3}$, respectively, when 20 $\mu g\ m^{-3}$ < ALWC < 60 $\mu g\ m^{-3}$. Notably, only aqSOA concentration continued to rise under high ALWC conditions (> 100 $\mu g\ m^{-3}$). This enhancement likely results from the formation of more water-soluble organic species, such as glyoxal and methylglyoxal, which are subsequently oxidized to aqSOA via aqueous-phase reactions in aerosol liquid water (Carlton et al., 2007; Ervens et al., 2011; Tan et al., 2012).

As shown in Fig. 4b, the mass fraction of aqSOA increased significantly from less than 5% at ALWC < 20 $\mu g\ m^{-3}$ to 17−22% at ALWC > 60 $\mu g\ m^{-3}$, accompanied by a corresponding decrease in the OOA fraction. In contrast, the contributions of POA (BBOA+CCOA+HOA) and SOA (OOA+aqSOA) remained relatively stable across different ALWC levels (58−68% and 32−42% for POA and SOA, respectively). This result suggested a more intensive formation of aqSOA than OOA via aqueous-phase reactions, although aqSOA might also be formed from OOA,

16

consistent with the recent studies in northwestern China (Zhao et al., 2019; Zhong et al., 2021).

Furthermore, f_{29} (CHO$^+$) increased from 0.010 to 0.227 as a function of ALWC (Fig. 4b). A pronounced rise in f_{29} from 0.055 to 0.210 occurred when ALWC increased from 60 µg m^{-3} to 100 µg m^{-3} ($p < 0.001$), tracking the concurrent increase in OA mass concentrations (13.2−109.1 µg m^{-3}). Previous laboratory analysis of organic standards have found that species without alcohol groups showed low f_{29} (< 0.05), while polyols and species with non-acid OH groups, common products of biomass-burning emissions, display high f_{29} values (0.05–0.15) (Canagaratna et al., 2015; Gilardoni et al., 2016; Zhao et al., 2014). This further supports the potential formation of organic compounds with hydroxyl groups (i.e., glyoxal and methylglyoxal) under high ALWC conditions. Overall, these results pointed to the fact that the observed aqSOA could be formed predominantly from biomass-burning emissions via aqueous-phase reactions, reinforcing the important role of BBOA in increasing PM$_{2.5}$ mass concentration.
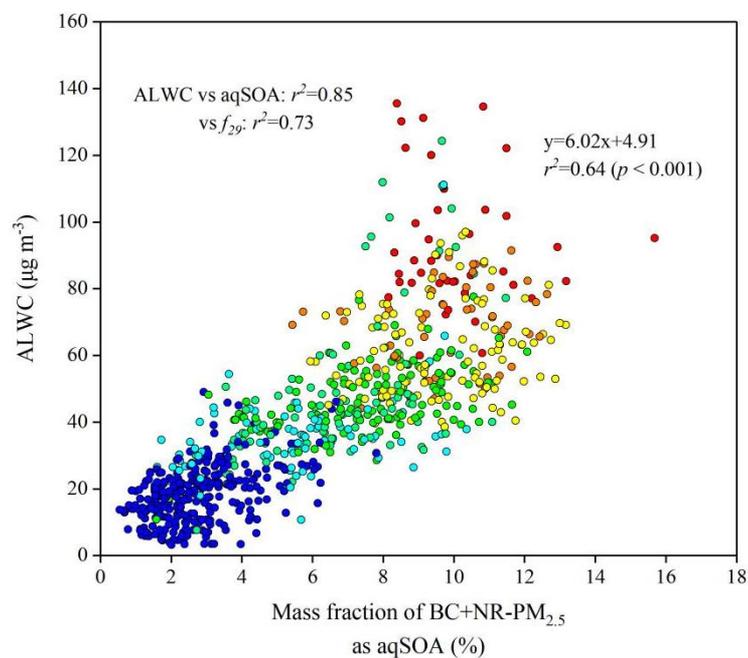
Figure 3. Scatter plot of the mass fraction of aqSOA in BC+NR-PM$_{2.5}$ versus ALWC colored by the f_{29} (normalized signal at m/z 29) during the campaign. f_{29} (mainly CHO$^+$) is a tracer for alcohol compounds and used to monitor the aqueous-phase oxidation of organic compounds (i.e., glyoxal).

删除[Mi]: research
删除[Mi]: northwest
删除[Mi]: Additionally
删除[Mi]: the increasing
删除[Mi]: was observed during the campaign
删除[Mi]: The values
删除[Mi]: of
删除[Mi]: significantly increased
删除[Mi]: consistent with
删除[Mi]: during the campaign (Fig. 4b)
删除[Mi]: According to the
删除[Mi]: , previous research
删除[Mi]: the spectra of standard organic
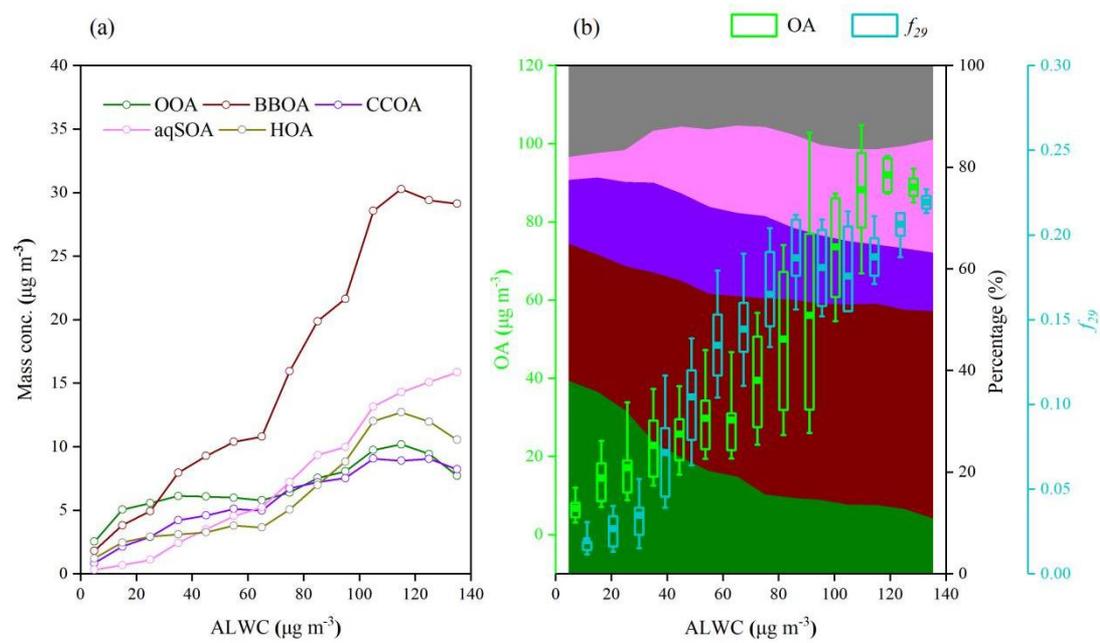删除[Mi]: high f_{29} values (0.05–0.15)
删除[Mi]: were found for
删除[Mi]: ed
删除[Mi]: from
删除[Mi]: highlighted
删除[Mi]: role
删除[Mi]: mass spectrum

442

Figure 4. Variations of **(a)** OA factors mass concentrations, and **(b)** OA mass concentrations, f_{29} (a tracer for alcohol compounds), and mass fraction of OA factors as a function of ALWC. Data were grouped into different bins according to a 10 µg m^{-3} increment of ALWC.

To identify the formation of aqSOA and its precursors under different PM$_{2.5}$ pollution levels, the relationships between aqSOA and BBOA or OOA mass concentrations, as well as key ion-fragment tracers, were analyzed separately during CP and PP. The correlation (r^2) between aqSOA and BBOA was stronger during PP (0.64) than during CP (0.54) ($p < 0.001$, Fig. 5a and c). Although both aqSOA and BBOA concentrations increased with rising ALWC during both periods, the correlations of ALWC with aqSOA and BBOA were relatively stronger during PP than during CP ($p < 0.001$). As shown in Fig. 5b and d, f_{29} was highly correlated with aqSOA formation during both CP and PP. A subset of data points with high aqSOA and OOA concentrations displayed relatively low f_{29} values (0.071−0.102) in Fig. 5d. For these points, the average value of f_{44} (normalized signal of m/z 44) (0.103 ± 0.024) was 1.3 times that of the overall dataset (0.080 ± 0.035) during PP, likely due to the formation of more-oxidized OOA under high ALWC values (> 80 µg m^{-3}) (Xu et al., 2017). Previous studies have found that f_{29} values for polyols and species with non-acid OH groups from biomass-burning emissions were typically lower than 0.15 (Canagaratna et al., 2015; Gilardoni et al., 2016; Zhao et al., 2014). Moreover, the

删除[Mi]: The d

删除[Mi]: with

删除[Mi]: ion

删除[Mi]: s

删除[Mi]: was performed, respectively

删除[Mi]:

删除[Mi]:

删除[Mi]: concentrations

删除[Mi]: higher

删除[Mi]: that

删除[Mi]:) (

删除[Mi]: T

删除[Mi]: the increase of

删除[Mi]: CP and PP

删除[Mi]: between

删除[Mi]: and

删除[Mi]: or

删除[Mi]: concentrations

删除[Mi]: that

删除[Mi]: show that

删除[Mi]: few

删除[Mi]: had

删除[Mi]: ,

删除[Mi]: while

删除[Mi]: mass spectrum

删除[Mi]: at

删除[Mi]: of these data points

删除[Mi]: point

删除[Mi]: . It was

删除[Mi]: in this study

删除[Mi]: research

删除[Mi]: the

删除[Mi]: of

mass fraction of aqSOA showed a stable increasing trend and remained elevated (from 18% to 22%) at ALWC > 80 μg m^{-3}, accompanied by a corresponding decrease in OOA (from 15% to 10%) (Fig. 4b). In contrast to OOA (p > 0.1), aqSOA concentration showed a strong positive correlation with ALWC (r^2 = 0.73, p < 0.001) when ALWC > 80 μg m^{-3} during PP. However, no such correlations were observed during CP (p > 0.1). Notably, a strong anticorrelation between aqSOA and OOA concentrations was observed during PP at ALWC > 80 μg m^{-3} when f_{29} > 0.15 (r^2 = 0.76, p < 0.001), but not during CP (p > 0.1) (Fig. 5b and d). These results indicated that aqSOA formation was more intensive than OOA at high ALWC levels during PP.

Previous research demonstrated that f_{44} could be used as a tracer for aged SOA, f_{43} (normalized signal at m/z 43) for POA and fresh SOA, and f_{60} (presence of anhydrosugars) for BBOA (Cubison et al., 2011; Ng et al., 2010). Additionally, m/z 44 and 43 are usually from different functional groups and their ratio changes as a function of atmospheric aging. The triangle plot of f_{44} versus f_{43} has been widely used to characterize OA evolution, while f_{44} versus f_{60} is commonly used to track the aging of BBOA (Ortega et al., 2013; Paglione et al., 2020; Xu et al., 2017; Xu et al., 2019). In this study, the bottom region of the triangle (Fig. 6) was dominated by BBOA, CCOA, and HOA, which exhibited low f_{44} (0.040, 0.017, and 0.016, respectively), indicating fresh, less-oxidized emissions. In contrast, the f_{44} of SOA factors (i.e., OOA and aqSOA) (0.118 and 0.117) were observably higher, reflecting their oxidized nature. The f_{44} of aqSOA was close to that observed in fogs (Gilardoni et al., 2016; Kim et al., 2019), highlighting the role of aqueous-phase reactions in this study. Moreover, the relative abundance of m/z 45 (mainly HCO_2^+), a tracer ion for carboxylic acids, was higher in the aqSOA spectrum than in the OOA spectrum (Fig. S9), consistent with previous findings that aqueous-phase reactions were important sources of oxygenated organic compounds, including organic acids (Ervens et al., 2011; Kim et al., 2019; McNeill, 2015; Sun et al., 2010; Yu et al., 2014). As shown in Fig. 6b, BBOA and aqSOA displayed higher f_{60} values (0.019 and 0.011) than CCOA (0.009) and HOA (0.008). The f_{60} value of OOA was 0.002, lower than the typical background level (0.003) observed in the atmospheric unaffected by biomass burning

(Cubison et al., 2011). The mass spectrometry feature of aqSOA, characterized by elevated f_{44} and f_{60} values, placed it in the schematic region of aged BBOA reported in previous studies (Cubison et al., 2011; Ortega et al., 2013). Additionally, BBOA contains abundant water-soluble organic compounds (WSOC) (i.e., sugars, phenols, and organic acids) that can efficiently form aqSOA via aqueous-phase reactions (i.e., oxidation and oligomerization reactions) (Ervens et al., 2011; Gilardoni et al., 2016; Lee et al., 2013; Lei et al., 2024; Li et al., 2020; Powelson et al., 2014). In contrast, OOA formation primarily relies on gas-phase oxidation of VOCs with high-reactivity (i.e., aromatics and long-chain alkanes by OH radicals, which have low concentrations in BBOA plumes (Akagi et al., 2011; Jimenez et al., 2009; Shrivastava et al., 2017; Yokelson et al., 2007). This suggested that BBOA acted as the important precursors for aqSOA instead of OOA via aqueous-phase reactions. These results were consistent with previous studies and most of the observed data fall within the triangle space (Bao et al., 2023; Kim et al., 2019; Paglione et al., 2020). It should be noted that these processes of aqSOA formation could be more intense and important during autumn due to elevated precursor concentrations (i.e., BBOA), ALWC, and RH values, though the underlying chemical pathways are robust and cam occur year-round (Bao et al., 2023; Tang et al., 2025; Zeng et al., 2025).

During PP, f_{44} values ranging from 0.022 to 0.140 (0.080 ± 0.035) were significantly higher than those during CP (0.021−0.150, 0.064 ± 0.019) ($p < 0.001$), while f_{43} was slightly lower with an average of 0.062 ± 0.027. Compared with CP (r^2 = 0.17, slope = −0.53), f_{44} showed a more pronounced inverse relationship with f_{43} during PP, characterized by a higher r^2 value (0.70) and a regression slope closer to −1 (−1.09). This pattern indicated a greater abundance of aged SOA in the atmosphere during PP (Fig. 6a and c). It should be noted that the data points of in the f_{44} − f_{43} space during PP fell within the upper boundary of the triangle region, with most points located outside the bottom boundary. These results suggested that less oxidized SOA were predominantly formed via aqueous-phase reactions instead of photochemical pathways during PP (Kim et al., 2019; Zhao et al., 2019). Moreover, points outside the bottom boundary of the triangle region, characterized by higher f_{44}

(> 0.05) and lower f_{43} (< 0.06), were associated with relatively higher ALWC during PP, a feature not observed during CP.

Here, the triangle plots of f_{44} versus f_{60} colored by ALWC under different $PM_{2.5}$ pollution levels were analyzed (Fig. 6b and d), when the link between aqSOA and BBOA was further stressed by a schematic representation of aged BBOA. With the exception of a few outliers, f_{60} values were consistently higher than 0.003, and most data points fell within the triangular region, suggesting a widespread influence of biomass burning on OA. During PP, f_{60} ranged from 0.005 to 0.019 (0.010 ± 0.004), similar to the range observed in CP (from 0.004 to 0.019, 0.010 ± 0.003). However, the correlation between f_{44} and f_{60} was higher during PP (r^2 = 0.72) than during CP (r^2 = 0.31) ($p < 0.001$). Moreover, data points within the schematic space of aged BBOA showed relatively higher ALWC compared with overall dataset during PP, a pattern that was not evident during CP.

Regional transport significantly influenced the aging of BBOA in the SCB. Previous studies have demonstrated that northeast winds prevail during autumn in this region, facilitating the transport of pollutants along the Dazhou→Guang'an→Hechuan pathway, and this northeast-southwest transport pathway had a significant impact on Chongqing (Peng et al., 2019; Wang et al., 2018). As shown in Fig. S11, air masses during the campaign predominantly originated from northeastern Chongqing, an area with widespread agricultural burning activities (He et al., 2015; Luo et al., 2020), and were transported over relatively short distances. Compared to other air mass clusters, the highest contribution and concentration of BBOA to total $PM_{2.5}$ were observed when air masses passed through northeastern Chongqing. The percentage of air mass trajectories that passed through biomass-burning-influenced regions was higher during PP (~57%) than CP (~35%). Unlike cluster 3 during CP, air masses originating from northeastern Chongqing (cluster 2) during PP showed significantly higher contributions and concentrations of BBOA (24.7%, 27.8 μg m^{-3}) and aqSOA (9.4%, 10.6 μg m^{-3}) than other clusters ($p < 0.001$). In addition, cluster 2 exhibited notably higher values of ALWC (93.7 μg m^{-3}), Abs$_{370,BrC,sec}$ (105.1 Mm^{-1}), f_{44} (0.113), and the

551 NO$_3$/SO$_4$ ratio (2.1, a tracer for BBOA aging (Liu et al., 2024; Zhang et al., 2025))

552 than other clusters during PP ($p < 0.001$). During PP, approximately 68% of the

553 trajectories in cluster 2 passed through biomass-burning-influenced regions, with

554 transport times to the sampling site ranging from 12 to 48 hours, consistent with the

555 typical timescale for aqueous-phase aging of biomass burning emissions reported in

556 earlier works (Cubison et al., 2011; Hennigan et al., 2010; Ortega et al., 2013; Zhu et

557 al., 2023). These results suggested that regional transported BBOA, primarily

558 originated from northeastern Chongqing, underwent aging to form aqSOA within

559 approximately 12 to 48 hours.

560

Figure 5. Scatter plots of aqSOA versus **(a, b)** BBOA and **(c, d)** OOA mass concentrations

colored by ALWC during clean period and polluted period. The size of the symbols in **(b)** and **(d)**

increases with the increase of the f_{29} value, which is a tracer for alcohol compounds.

删除[Mi]: between

删除[Mi]: and

删除[Mi]: . This time frame is

删除[Mi]: previous research on the

删除[Mi]: process

删除[Mi]: o

删除[Mi]: f

删除[Mi]: and

删除[Mi]: ed
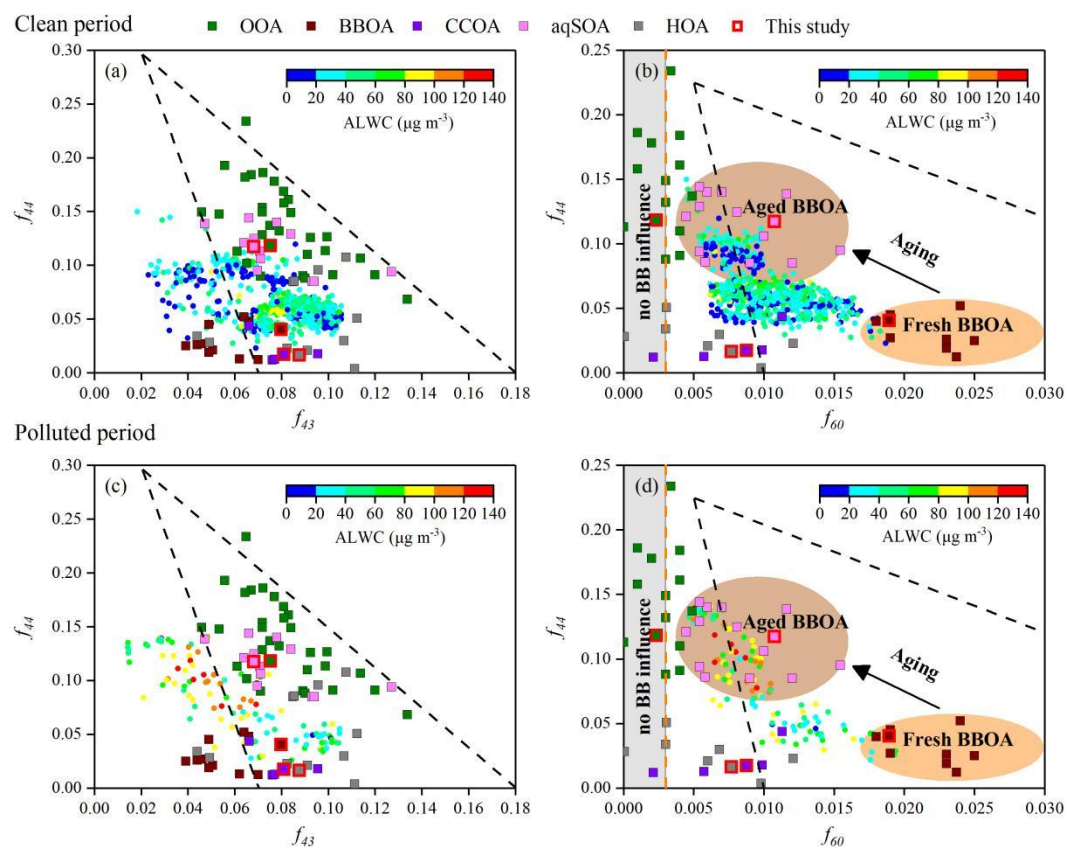
Figure 6. Triangle plots of **(a, c)** f_{44} (normalized mass spectrum signal at m/z 44) versus f_{43} (normalized mass spectrum signal at m/z 43), and **(b, d)** f_{44} versus f_{60} (normalized mass spectrum signal at m/z 60) colored by ALWC (circles) during clean period and polluted period. The dashed lines in **(a)** and **(c)** were derived from Ng et al. (2010) and used to follow the aging of OA components in the atmosphere. The background space ($f_{60} < 0.003$) without biomass burning influence was also shown by the grey shaded area. The background value of secondary aged OA (brown dashed line) and the black dashed lines characterizing the aging of BBOA in **(b)** and **(d)** were derived from Cubison et al. (2011). The data points (squares) included the measurements in this study (bordered in red) and previous research (Bao et al., 2023; Gilardoni et al., 2016; Kim et al., 2019; Ng et al., 2011a; Paglione et al., 2020; Xu et al., 2015; Xu et al., 2017; Xu et al., 2019; Zhao et al., 2017; Zhao et al., 2019). f_{43} (mainly $C_2H_3O^+$) is a tracer for POA and fresh SOA. f_{44} is a proxy of the OA oxygenation degree and used as a tracer for aged SOA. f_{60} is a proxy of anhydrosugars emitted from biomass burning.

删除[Mi]: characterising

3.3 Evolution of BrC Absorption

Previous research indicated that OA from both fresh and aged biomass-burning emissions exhibited light absorption across UV to Vis range, with significantly higher AAE value than BC, and might contribute to a net positive radiative forcing (Laskin et al., 2015). In this work, the absorption properties of BrC and their relationships with the five OA factors were analyzed. The values of $Abs_{\lambda,BrC,pri}$ and $Abs_{\lambda,BrC,sec}$ were obtained by MRS method, and MLR method was used to estimate Abs of each OA factor at each wavelength (SI Text S3 and S4). The average value of $Abs_{370,BrC}$ was 42.4 ± 28.5 Mm^{-1} (accounting for 49.2% of Abs_{370}), much higher than $Abs_{660,BrC}$ (2.6 ± 1.3 Mm^{-1}, 10.5%), suggesting high absorption efficiency for BrC in the near-UV region. From 370 nm to 660 nm, $Abs_{\lambda,BrC,pri}$ and $Abs_{\lambda,BrC,sec}$ accounted for 56.8%−72.5% and 27.5%−43.2% of $Abs_{\lambda,BrC}$, respectively, indicating that primary emissions were the dominant contributors to BrC absorption (Fig. S13). However, the contribution of $Abs_{\lambda,BrC,sec}$ to $Abs_{\lambda,BrC}$ increased with wavelength, suggesting that the impact on Abs_{BrC} from SOA should not be ignored. The following analysis demonstrates that aqSOA formed from aged BBOA contributed substantially to the BrC budget and exhibited strong light absorption across UV to Vis range.

Data at 370 nm, which exhibit higher signal-to-noise ratios and a greater contribution of Abs_{BrC}, were selected to further analyze the correlations of BrC absorption with various OA components. As described in section 2.3.3, the Abs of the five OA factors at each wavelength were obtained by MLR method (Table S2). The contributions of BBOA ($Abs_{370,BBOA}$) and aqSOA ($Abs_{370,aqSOA}$) to $Abs_{370,BrC}$ were 51.9% and 16.4%, respectively, higher than those of CCOA ($Abs_{370,CCOA}$, 11.5%), HOA ($Abs_{370,HOA}$, 9.1%), and OOA ($Abs_{370,OOA}$, 11.1%). This pattern is consistent with the higher MAC values of BBOA and aqSOA (Fig. S15).

Figure S16 presents correlations between $Abs_{370,BrC}$ and the mass concentrations of OOA, BBOA, CCOOA, aqSOA, HOA, and the tracer ion m/z 60 (ion fragments tracers of BBOA). $Abs_{370,BrC}$ showed the strongest positive correlations with BBOA and m/z 60 ($r^2 = 0.77$, $p < 0.001$), followed by aqSOA ($r^2 = 0.69$, $p < 0.001$). In

contrast, correlations with HOA ($r^2 = 0.36$), CCOA ($r^2 = 0.25$), and OOA ($r^2 = 0.09$, $p > 0.1$) were much weaker. Among all OA factors (excluding BBOA), aqSOA contributed relatively more to $Abs_{370,BrC}$ (Table S2), and also displayed a stronger correlation with $Abs_{370,BrC}$. These results might be related to the formation of aqSOA from aged BBOA via aqueous-phase reactions. Gilardoni et al. (2016) demonstrated that aqSOA derived from aged BBOA via aqueous-phase reactions in the ambient atmosphere contributed to the BrC budget and exhibited slightly higher $AAE_{467-660}$ (AAE of aerosols from 467 nm to 660 nm) values than fresh or processed biomass-burning emissions in laboratory experiments.

The MAC values of the five resolved OA components (equivalent to coefficients a–e in the MLR method) at different wavelengths were shown in Fig. S15. At 370 nm, BBOA showed the highest MAC (2.37 m^2 g^{-1}), followed by aqSOA (1.23 m^2 g^{-1}), indicating that oxidation of BBOA to aqSOA reduced light absorption at shorter wavelengths. Previous research found that the MAC of BBOA at 365 nm was twice that of SOA, which was associated with the water-soluble BrC (Lorenzo et al., 2017; Washenfelder et al., 2015). The AAE values of the OA factors, calculated by a power-law fitting of their Abs from 370 nm to 660 nm (Qin et al., 2018; Wang et al., 2019b), were shown in Fig. S15. It should be noted that aqSOA had the lowest $AAE_{370-660,aqSOA}$ value (3.54), while BBOA had the highest $AAE_{370-660,BBOA}$ value (4.93). Moreover, the contribution of aqSOA to Abs_{BrC} increased from 16.4% at 370 nm to 26.7% at 660 nm, while the contribution of BBOA decreased from 51.9% to 39.1% over the same wavelength range. These findings suggested aqSOA formed from aged BBOA might play an important role in the light absorption of BrC across the UV to Vis range.

Figure 7 shows a ternary contour map that quantifies the contributions of BBOA, CCOA, and HOA to $Abs_{370,BrC,pri}$. A strong positive correlation ($p < 0.001$) and a steep linear regression slope (1.80) were observed between BBOA mass concentration and $Abs_{370,BrC,pri}$. Among these POA factors, high mass fractions of BBOA relative to POA were consistent with high values of $Abs_{370,BrC,pri}$ (Fig. 7a). For example, most data points with $Abs_{370,BrC,pri}$ higher than 49.1 Mm^{-1} (90th percentile of $Abs_{370,BrC}$) fell

25

within the region of high BBOA/POA values (> 0.5). Moreover, $Abs_{370,BrC,pri}$ increased significantly with rising BBOA and m/z 60 mass concentrations, exhibiting higher correlation coefficients (r^2 = 0.63 and 0.55) than HOA (r^2 = 0.19) and CCOA (r^2 = 0.14) (Fig. 7b). These results indicated the major contribution of BBOA to primary BrC light absorption at 370 nm.

To understand the relationship between secondary BrC absorption and its chromophores, the correlation between $Abs_{370,BrC,sec}$ and the mass concentrations of SOA factors was analyzed. As shown in Fig. S17, $Abs_{370,BrC,sec}$ increased significantly with rising aqSOA concentration (r^2 = 0.44, p < 0.001), and high $Abs_{370,BrC,sec}$ values were associated with elevated ALWC. In contrast, no such relationship was found for OOA (p > 0.1). The slope of the linear regression between aqSOA mass concentrations and $Abs_{370,BrC,sec}$ (3.50) was steeper than that for OOA (Fig. S17), and the MAC values of aqSOA was also higher across UV to Vis range (Fig. S15).

To further characterize the evolution of secondary BrC absorption, $Abs_{370,BrC,sec}$ was normalized by ΔCO (background-corrected CO mixing ratios) to minimize the effect of boundary layer height (Fig. 8) (DeCarlo et al., 2010). Here, the background CO value (400 ppb) was defined as the lowest 1.25th percentile of CO values during the campaign (Kondo et al., 2006). Figure 8 shows that the ratios of $Abs_{370,BrC,sec}/\Delta CO$ increased with both aqSOA concentration and ALWC from 17:00 to 03:00 LT (r^2 = 0.63, 0.57, p < 0.001), while $Abs_{370,BrC,pri}/\Delta CO$ decreased slightly with increasing BBOA and m/z 60 concentrations over the same period (r^2 = 0.35, 0.33, p < 0.001). Additionally, the mass concentrations of NO_3, NH_4, and NO_2 from 17:00 to 03:00 LT were 1.2, 1.2, and 1.3 times those from 04:00 to 16:00 LT, respectively. These results were consistent with previous winter observations in the SCB (Peng et al., 2025; Wu et al., 2024).

As discussed in section 3.2, SOA with hydroxyl groups (i.e., glyoxal and methylglyoxal) could form from aged BBOA via aqueous-phase reactions under high ALWC. Previous studies have shown that oligomers (involving two glyoxal molecules) formed via aqueous reactions of glyoxal with NH_3, which contain C=C or C=N bonds, exhibit strong absorption at near-UV (Laskin et al., 2015; Lee et al., 2013;

Nozière et al., 2009; Powelsonet al., 2014). This suggested that secondary BrC chromophores with strong absorption at 370 nm were formed under high ALWC from 17:00 to 03:00 LT, which might be related to aqSOA generated from aged BBOA via aqueous-phase reactions. The low values of $Abs_{370,BrC,sec}/\Delta CO$ at 12:00−14:00 LT could be related to photolysis and/or photooxidation causing BrC photobleaching (Sareen et al., 2013; Zhao et al., 2015). Overall, our findings suggested that aqSOA formed from biomass-burning emissions contributed importantly to BrC absorption, especially at night during the campaign.

Previous studies indicated that biomass-burning activity is negligible in summer, and although it may also experience in spring and winter, its intensity is typically less intense than in autumn (Chen et al., 2014; Chen et al., 2017; Tao et al., 2014; Yang et al., 2019). For example, Tao et al. (2014) found that the contribution of biomass burning to $PM_{2.5}$ during autumn (19 ± 11%) was significantly higher than in other seasons. Meanwhile, the highest fraction of organic matter (OM) in $PM_{2.5}$ was also observed during autumn (33.4%), with biomass burning as the dominant contributor. Additionally, the concentration of BBOA and its fraction in OA during autumn in this study (8.6 ± 7.7 μg m^{-3} and 34.8 ± 11.2%, respectively) were respectively higher than those observed during summer (0.41 μg m^{-3} and 5.7%, respectively) (Zeng et al., 2025) and winter in the SCB (Tang et al., 2025; Zhang et al., 2023) (Table S1). It should be noted that the ALWC during autumn in this study (41.6±24.9 μg m^{-3}) was substantially higher than that reported for summer (18.6 ± 35.3 μg m^{-3}) (Zeng et al., 2025) and winter (27.4±9.7 μg m^{-3}) (Tang et al., 2025) in the SCB. Wang et al. (2018) observed that RH values at Chengdu and Chongqing in autumn were also higher than those in other seasons. Previous research indicated that while aqueous-chemistry pathways in spring were comparable to those in autumn, photochemical bleaching of BrC was potentially stronger in spring (Wang et al., 2019a). Although winter features lower biomass-burning emissions, secondary BrC could still form from BBOA through aqueous-phase reactions under high NO_x and NH_4 concentrations and stagnant nighttime conditions, as observed during winter in the SCB (Peng et al., 2025; Wu et al., 2024). In summer, elevated temperature and O_x (O_x = NO_2 +O_3) levels

删除[Mi]: the

删除[Mi]: the

删除[Mi]: the

删除[Mi]: the

删除[Mi]: we

删除[Mi]: might be important for

删除[Mi]: also provided evidence

删除[Chao]: spring

删除[Chao]: similar but less intense biomass-burning activity

删除[Chao]: though

删除[Chao]: , with comparable aqueous aqueous-chemistry pathways but though potentially increasedstronger photochemical bleaching of BrC (Wang et al., 2019a).

删除[Mi]: T

删除[Mi]: likely

删除[Mi]: ed

删除[Mi]: after sunset

删除[Mi]: E

could enhance photochemical oxidation, promoting secondary BrC formation while also intensifying BrC photobleaching (Wu et al., 2024). In summary, while secondary BrC can form from BBOA through aqueous-phase reactions in all seasons in the SCB (with the possible exception of spring), the elevated ALWC and BBOA concentrations during autumn are particularly favorable for its aqueous-phase formation.

$AAE_{370-880}$ is another key parameter for characterizing aerosol absorption properties. Figure 9 displays its correlations with the mass fraction of aqSOA (f_{aqSOA}) and BBOA (f_{BBOA}) to OA, and the BC-to-OA ratio. During the campaign, a strong positive correlation ($r^2 = 0.49$, $p < 0.001$) was observed between $AAE_{370-880}$ and f_{aqSOA}, with $AAE_{370-880}$ reaching values up to 2.65. In contrast, $AAE_{370-880}$ increased only slightly with rising f_{BBOA} ($r^2 = 0.21$, $p < 0.001$) (Fig. 9a and c). AAE was calculated using a power-law fitting of aerosol absorption values (Qin et al., 2018; Wang et al., 2019b). While BC concentration was linearly dependent on Abs_{BC}, OA concentration did not follow the same pattern with Abs_{BrC}. The mixing state of BC and OA, influenced by combustion conditions, can also affect AAE. Previous studies have shown that biomass-burning emissions can impact absorption properties, which is reflected in the relationship between AAE and the BC-to-OA ratio (a measure of the combustion conditions) (Lu et al., 2015; Saleh et al., 2014). Thus, the relationship observed in Fig. 9b reflected the influence of biomass-burning emissions during this campaign. The parameterized curve obtained here (black) was consistent with prior research (red) derived for wavelengths from 370 nm to 880 nm (Lu et al., 2015). When 950 nm was used as the highest wavelength instead of 880 nm, $AAE_{370-950}$ values differed by less than 10% from $AAE_{370-880}$. It should be noted that data points with high $AAE_{370-880}$ generally corresponded to low BC-to-OA ratios and large f_{aqSOA} values. Moreover, the average value of $AAE_{370-880}$ observed in this study (1.95) was higher than $AAE_{370-950}$ observed in the laboratory experiments on fresh and photochemically aged biomass-burning emissions (i.e., 1.38 and 1.48 for fresh oak and pocosin pine, 1.42 and 1.73 for aged oak and pocosin pine) (Saleh et al., 2013).

725
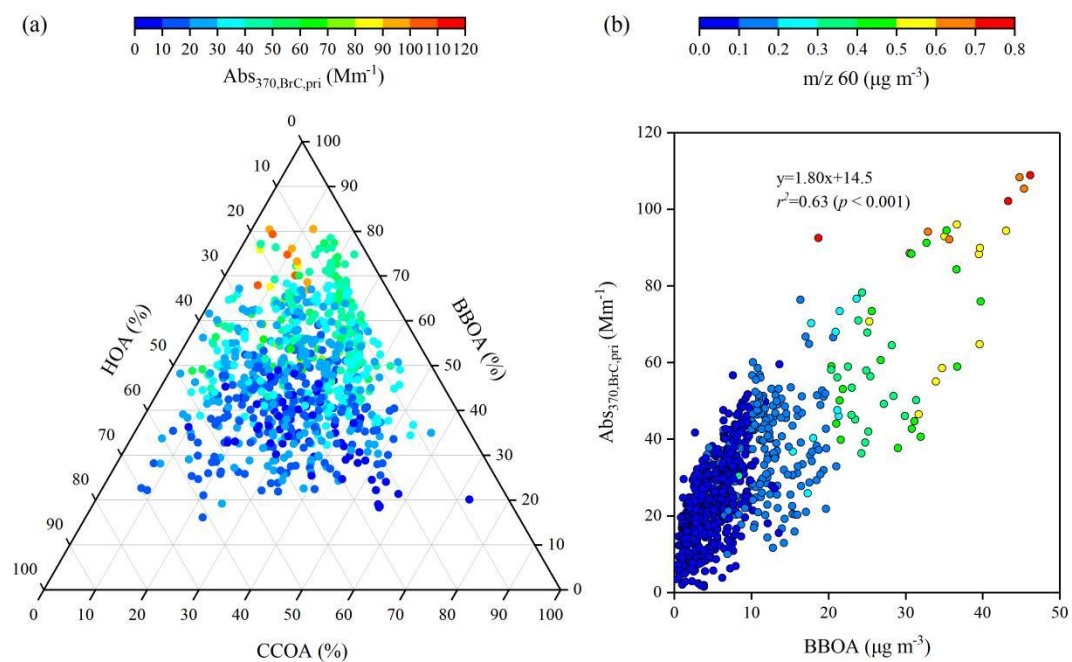
Figure 7. (a) Ternary diagram for the mass fractions of BBOA, CCOA, and HOA in POA colored

by $Abs_{370,BrC,pri}$, and **(b)** scatter plot of BBOA mass concentrations versus $Abs_{370,BrC,pri}$ colored by

m/z 60 mass concentrations.

729
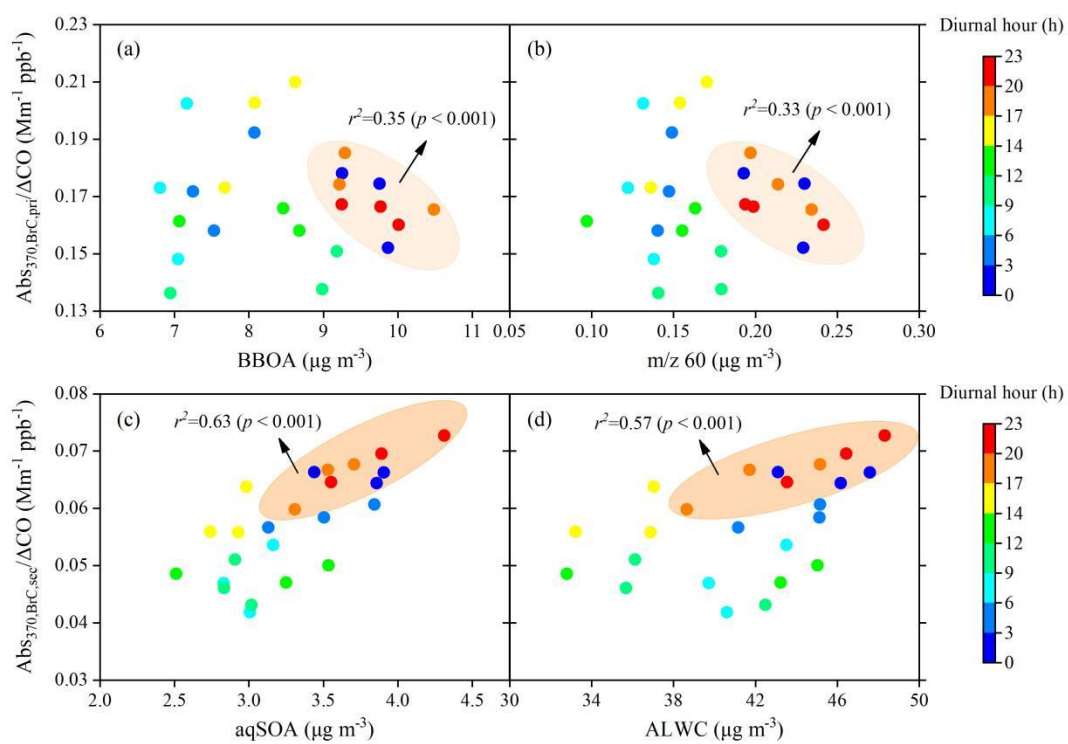
Figure 8. Scatter plots of $Abs_{370,BrC,pri}/\Delta CO$ versus **(a, b)** BBOA and m/z 60 mass concentrations and $Abs_{370,BrC,sec}/\Delta CO$ versus **(c, d)** aqSOA and ALWC colored by the local time.
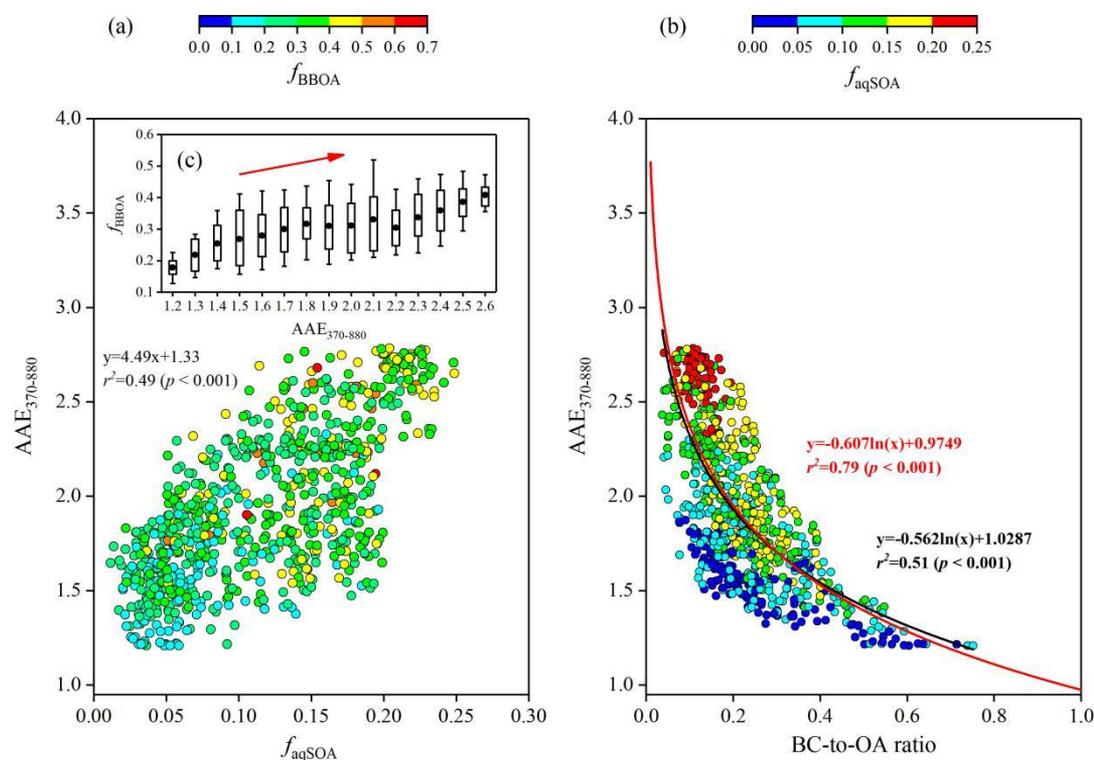
Figure 9. Relationship between **(a)** $AAE_{370-880}$ and the mass fraction of aqSOA ($f_{aqSOA} =$ aqSOA/OA) colored by the mass fraction of BBOA ($f_{BBOA} =$ BBOA/OA), and **(b)** BC-to-OA ratios colored by f_{aqSOA}. **(c)** Variations of f_{BBOA} as a function of $AAE_{370-880}$. The red curve in **(b)** was the best fit curve to data taken from Lu et al. (2015) and described the Abs of fresh and aged BBOA.

4 Conclusions

This study conducted comprehensive real-time measurements of the light absorption properties and chemical composition of carbonaceous aerosols during autumn in the Sichuan Basin, China. The findings provided direct ambient evidence that aqueous secondary organic aerosol (aqSOA) formed from aged biomass-burning emissions under high aerosol liquid water content (ALWC > 60 μg m^{-3}) conditions significantly contributes to both aerosol pollution and light absorption. Organic aerosol (OA) was the dominant component of PM$_{2.5}$ (46.6 ± 10.7%), and exhibited

删除[Mi]: demonstrating

删除[Mi]: the

删除[Mi]:

删除[Mi]: identified as

30

strong absorption at UV wavelengths ($Abs_{370,BrC}$ = 42.4 ± 28.5 Mm^{-1}). During pollution periods (PP), aqSOA (averaged at 7.6 µg m^{-3}) contributed on average 14.1% to OA, exhibiting enhanced oxidation (f_{29} = 0.141 ± 0.062, f_{44} = 0.080 ± 0.035) and substantial light absorption characteristics ($Abs_{370,BrC}$ = 91.6 Mm^{-1}, $AAE_{370–880}$ = 2.1). Additionally, less-oxidized aqSOA, formed predominantly via aqueous-phase reactions, instead of gas-phase photochemical oxidations of their precursors, played a key role in the dynamic evolution of haze pollution during PP. Backward trajectory analysis further revealed that regionally transported BBOA, originated mainly from northeastern Chongqing, underwent aqueous-phase aging to aqSOA within approximately 12 to 48 hours. These results underscore that aqueous-phase reactions of BBOA—particularly during the transport of biomass-burning plumes—converts primary emissions into strongly light-absorbing aqSOA, thereby substantially influencing regional haze formation and radiative forcing.

Our findings align with previous laboratory studies on biomass-burning BrC formation (Lu et al., 2015; Powelsonet al., 2014), while providing novel ambient quantification of these processes under realistic atmospheric conditions. The parameterized curve of $AAE_{370–880}$ versus BC-to-OA ratios in this study was consistent with the previous laboratory research on biomass-burning emissions. The mean $AAE_{370–880}$ observed in this study (1.95) were higher than values reported for fresh and photochemically aged biomass-burning emissions in laboratory experiments (Saleh et al., 2013), and increased significantly with rising f_{aqSOA} (r^2 = 0.49, p < 0.001). Additionally, elevated $Abs_{370,BrC,sec}$ values coincided with high ALWC, NO_3, and NH_4 levels and correlated strongly with aqSOA concentration (r^2 = 0.44, p < 0.001). These results suggest that aqueous-phase reactions of BBOA under high-NO_x and high-NH_4 conditions produce secondary BrC with particularly strong light absorption. It should be noted that seasonal variations in biomass-burning emissions and the associated chemical processing of carbonaceous aerosols must be adequately represented in climate and air quality models. This is critical to avoid underestimating aerosol impacts in autumn and overestimating them in other seasons. The campaign was conducted during autumn, when biomass-burning activity is intense, and thus may not

31

775 fully represent aerosol processes in other seasons. The relative uncertainty of Abs_{BrC}
776 at 370 nm, resulting from the choice of AAE_{BC}, ranged from −112% to 42%.
777 Nevertheless, our results underscore the importance of aqueous-phase processing in
778 transforming biomass-burning emissions, with important implications for climate and
779 air quality modeling. The substantial contribution of aqSOA to both aerosol mass and
780 light absorption highlights the need for improved representation of aqueous processes
781 in models. The linkages established here among aging timescales, transport pathways,
782 and aqSOA formation provide a transferable framework for understanding aqSOA
783 processing in other humid regions influenced by biomass burning. In general, research
784 on BrC chromophores is still at an early stage, and more studies that quantitatively
785 link the chemical composition and light absorption properties of BrC chromophores to
786 biomass-burning emissions across different seasons are necessary to improve our
787 understanding of their climatic and environmental effects. Future research should
788 prioritize molecular-level characterization of aqSOA precursors and products,
789 quantification of aqueous reaction rates under ambient conditions, and multi-scale
790 modeling to assess regional climate impacts. This study highlights that aqueous
791 processes play an important role in the evolution of biomass-burning emissions and
792 should be adequately considered in both air quality budgets and climate forcing
793 balance on a global scale.

794

795 **Data availability.** The data generated and analysed in this study are available from
796 https://doi.org/10.5281/zenodo.18635386 (Peng et al., 2026).

797

798 **Author contributions.** CZ, CP, YD, and ZL designed the experiments. Data analysis
799 and interpretation were performed by CP, ZT, HT, KZ, ZL, and GS. CP, XY, and MT
800 wrote the paper. ZT, YC, XL, LZ, YC, and YF contributed to the paper with useful
801 scientific discussions or comments.

802

803 **Competing interests.** The authors declare that they have no conflict of interest.

804

删除[Mi]: range

删除[Mi]:

删除[Mi]: was [

删除[Mi]: , +

删除[Mi]:] at 370 nm due to the choice of AAE_{BC}

删除[Mi]: O

删除[Mi]: significant

删除[Mi]: between

删除[Mi]: in this study

删除[Chao]: 10.5281/zenodo.14626304

删除[Chao]: 5

References

Akagi, S. K., Yokelson, R. J., Wiedinmyer, C., Alvarado, M. J., Reid, J. S., Karl, T., Crounse, J. D., and Wennberg, P. O.: Emission factors for open and domestic biomass burning for use in atmospheric models, Atmos. Chem. Phys., 11, 4039−4072, https://doi.org/10.5194/acp-11-4039-2011, 2011.

Alfarra, M. R., Prévôt, A. S. H., Szidat, S., Sandradewi, J., Sandradewi, S., Lanz, V. A., Schreiber, D., Mohr, M., and Baltensperger, U.: Identification of the Mass Spectral Signature of Organic Aerosols from Wood Burning Emissions, Environ. Sci. Technol., 41, 5770−5777, https://doi.org/10.1021/es062289b, 2007.

Bahreini, R., Ervens, B., Middlebrook, A. M., Warneke, C., de Gouw, J. A., DeCarlo, P. F., Jimenez, J. L., Brock, C. A., Neuman, J. A., Ryerson, T. B., Stark, H., Atlas, E., Brioude, J., Fried, A., Holloway, J. S., Peischl, J., Richter, D., Walega, J., Weibring, P., Wollny, A. G., and Fehsenfeld, F. C.: Organic Aerosol Formation in Urban and Industrial Plumes Near Houston and Dallas, Texas, J. Geophys. Res.: Atmos., 114, D00F16, doi:10.1029/2008JD011493, 2009.

Bao, Z. E., Liu, Y. L., Meng, L. S., Han, Y., Tian, M., Shi, G. M., Wang, Q. Y., Huang, Y., Peng, C., Luo, B., Zhang, W., Wang, H. B., Cao, J. J., Yang, F. M., and Chen, Y.: Evaluating the effects of biomass burning on severe haze formation in a megacity of Sichuan Basin, Southwestern China, J. Geophys. Res.: Atmos., 130, e2024JD042516, https://doi.org/10.1029/ 2024JD042516, 2025.

Bao, Z. E., Zeng, X. L., Zhou, J. W., Yang, F. M., Lu, K. D., Zhai, C. Z., Li, X., Feng, M., Tan, Q. W., and Chen, Y.: Evolution of black carbon and brown carbon during summertime in Southwestern China: An assessment of control measures during the 2023 Chengdu Summer World University Games, Environ. Pollut., 357, 124467, https://doi.org/10.1016/j.envpol.2024.124467, 2024.

Bao, Z. E., Zhang, X. Y., Li, Q., Zhou, J. W., Shi, G. M., Zhou, L., Yang, F. M., Xie, S. D., Zhang, D., Zhai, C. Z., Li, Z. L., Peng, C., and Chen, Y.: Measurement report: Intensive biomass burning emissions and rapid nitrate formation drive severe haze formation in the Sichuan Basin, China – insights from aerosol mass spectrometry, Atmos. Chem. Phys., 23, 1147−1167, https://doi.org/10.5194/acp-23-1147-2023,

839   2023.

840   Canagaratna, M. R., Jayne, J. T., Jimenez, J. L., Allan, J. D., Alfarra, M. R., Zhang, Q.,

841   Onasch, T. B., Drewnick, F., Coe, H., Middlebrook, A., Delia, A., Williams, L. R.,

842   Trimborn, A. M., Northway, M. J., DeCarlo, P. F., Kolb, C. E., Davidovits, P., and

843   Worsnop, D. R.: Chemical and microphysical characterization of ambient aerosols

844   with the aerodyne aerosol mass spectrometer, Mass Spectrom. Rev., 26, 185−222,

845   https://doi.org/10.1002/mas.20115, 2007.

846   Canagaratna, M. R., Jimenez, J. L., Kroll, J. H., Chen, Q., Kessler, S. H., Massoli, P.,

847   Hildebrandt Ruiz, L., Fortner, E., Williams, L. R., Wilson, K. R., Surratt, J. D.,

848   Donahue, N. M., Jayne, J. T., and Worsnop, D. R.: Elemental ratio measurements

849   of organic compounds using aerosol mass spectrometry: characterization,

850   improved calibration, and implications, Atmos. Chem. Phys., 15, 253−272,

851   https://doi.org/10.5194/acp-15-253-2015, 2015.

852   Canonaco, F., Crippa, M., Slowik, J. G., Baltensperger, U., and Prévôt, A. S. H.: SoFi,

853   an IGOR-based interface for the efficient use of the generalized multilinear engine

854   (ME-2) for the source apportionment: ME-2 application to aerosol mass

855   spectrometer   data,   Atmos.   Meas.   Tech.,   6,   3649−3661,

856   https://doi.org/10.5194/amt-6-3649-2013, 2013.

857   Carlton, A. G., Turpin, B. J., Altieri, K. E., Seitzinger, S., Reff, A., Lim, H. J., and

858   Ervens, B.: Atmospheric oxalic acid and SOA production from glyoxal: results of

859   aqueous   photooxidation   experiments,   Atmos.   Environ.,   41,   7588−7602,

860   https://doi.org/10.1016/j.atmosenv.2007.05.035, 2007.

861   Chen, C. R., Zhang, H. X., Yan, W. J., Wu, N. N., Zhang, Q., and He, K. B.: Aerosol

862   water content enhancement leads to changes in the major formation mechanisms of

863   nitrate and secondary organic aerosols in winter over the North China Plain,

864   Environ. Pollut., 287, 117625, https://doi.org/10.1016/j.envpol.2021.117625, 2021.

865   Chen, Y., Tian, M., Huang, R. J., Shi, G. M., Wang, H. B., Peng, C., Cao, J. J., Wang,

866   Q. Y., Zhang, S. M., Guo, D. M., Zhang, L. Y., and Yang, F. M.: Characterization of

867   urban amine-containing particles in southwestern China: seasonal variation, source,

868   and   processing,   Atmos.   Chem.   Phys.,   19,   3245−3255,

869 https://doi.org/10.5194/acp-19-3245-2019, 2019.

870 Chen, Y., Xie, S. D., Luo, B., and Zhai, C. Z.: Characteristics and origins of

871 carbonaceous aerosol in the Sichuan Basin, China, Atmos. Environ., 94, 215−223,

872 https://doi.org/10.1016/j.atmosenv.2014.05.037, 2014.

873 Chen, Y., Xie, S. D., Luo, B., and Zhai, C. Z.: Particulate pollution in urban

874 Chongqing of southwest China: Historical trends of variation, chemical

875 characteristics and source apportionment, Sci. Total Environ., 584−585, 523−534,

876 https://doi.org/10.1016/j.scitotenv.2017.01.060, 2017.

877 Coen, M. C., Weingartner, E., Apituley, A., Ceburnis, D., Fierz-Schmidhauser, R.,

878 Flentje, H., Henzing, J. S., Jennings, S. G., Moerman, M., Petzold, A., Schmid, O.,

879 and Baltensperger, U.: Minimizing light absorption measurement artifacts of the

880 Aethalometer: Evaluation of five correction algorithms, Atmos. Meas. Tech., 3,

881 457−474, https://doi.org/10.5194/amt-3-457-2010, 2010.

882 Cubison, M. J., Ortega, A. M., Hayes, P. L., Farmer, D. K., Day, D., Lechner, M. J.,

883 Brune, W. H., Apel, E., Diskin, G. S., Fisher, J. A., Fuelberg, H. E., Hecobian, A.,

884 Knapp, D. J., Mikoviny, T., Riemer, D., Sachse, G. W., Sessions, W., Weber, R. J.,

885 Weinheimer, A. J., Wisthaler, A., and Jimenez, J. L.: Effects of aging on organic

886 aerosol from open biomass burning smoke in aircraft and laboratory studies, Atmos.

887 Chem. Phys., 11, 12049−12064, https://doi.org/10.5194/acp-11-12049-2011, 2011.

888 DeCarlo, P. F., Ulbrich, I. M., Crounse, J., de Foy, B., Dunlea, E. J., Aiken, A. C.,

889 Knapp, D., Weinheimer, A. J., Campos, T., Wennberg, P. O., and Jimenez, J. L.:

890 Investigation of the Sources and Processing of Organic Aerosol over the Central

891 Mexican Plateau from Aircraft Measurements during MILAGRO, Atmos. Chem.

892 Phys., 10, 5257−5280, https://doi.org/10.5194/acp-10-5257-2010, 2010.

893 Drinovec, L., Močnik, G., Zotter, P., Prévôt, A. S. H., Ruckstuhl, C., Coz, E.,

894 Rupakheti, M., Sciare, J., Müller, T., Wiedensohler, A., and Hansen, A. D. A.: The

895 "dual-spot" Aethalometer: an improved measurement of aerosol black carbon with

896 real-time loading compensation, Atmos. Meas. Tech., 8, 1965−1979,

897 https://doi.org/10.5194/amt-8-1965-2015, 2015.

898 Drozd, G. T. and McNeill, V. F.: Organic matrix effects on the formation of

light-absorbing compounds from α-dicarbonyls in aqueous salt solution, Environ. Sci.: Processes Impacts, 16, 741−747, https://doi.org/10.1039/c3em00579h, 2014.

Elser, M., Huang, R. J., Wolf, R., Slowik, J. G., Wang, Q. Y., Canonaco, F., Li, G. H., Bozzetti, C., Daellenbach, K. R., Huang, Y., Zhang, R. J., Li, Z. Q., Cao, J. J., Baltensperger, U., El-Haddad, I., and Prévôt, A. S. H.: New insights into PM$_{2.5}$ chemical composition and sources in two major cities in China during extreme haze events using aerosol mass spectrometry, Atmos. Chem. Phys., 16, 3207−3225, https://doi.org/10.5194/acp-16-3207-2016, 2016.

Ervens, B., Turpin, B. J., and Weber, R. J.: Secondary organic aerosol formation in cloud droplets and aqueous particles (aqSOA): a review of laboratory, field and model studies, Atmos. Chem. Phys., 11, 11069−11102, https://doi.org/10.5194/acp-11-11069-2011, 2011.

Feng, Z., Liu, Y., Zheng, F., Yan, C., Fu, P., Zhang, Y., Lian, C., Wang, W., Cai, J., Du, W., Chu, B., Wang, Y., Kangasluoma, J., Bianchi, F., Petäjä, T., and Kulmala, M.: Highly oxidized organic aerosols in Beijing: Possible contribution of aqueous-phase chemistry, Atmos. Environ., 273, 118971, https://doi.org/10.1016/j.atmosenv.2022.118971, 2022.

Fountoukis, C. and Nenes, A.: ISORROPIA II: a computationally efficient thermodynamic equilibrium model for K$^+$–Ca^{2+}–Mg^{2+}–NH$_4^+$–Na$^+$–SO$_4^{2-}$–NO$_3^-$–Cl$^-$–H$_2$O aerosols, Atmos. Chem. Phys., 7, 4639−4659, https://doi.org/10.5194/acp-7-4639-2007, 2007.

Fröhlich, R., Cubison, M. J., Slowik, J. G., Bukowiecki, N., Prévôt, A. S. H., Baltensperger, U., Schneider, J., Kimmel, J. R., Gonin, M., Rohner, U., Worsnop, D. R., and Jayne, J. T.: The ToF-ACSM: a portable aerosol chemical speciation monitor with TOFMS detection, Atmos. Meas. Tech., 6, 3225−3241, https://doi.org/10.5194/amt-6-3225-2013, 2013.

Gilardoni, S., Massoli, P., Paglione, M., Giulianelli, L., Carbone, C., Rinaldi, M., Decesari, S., Sandrini, S., Costabile, F., Gobbi, G. P., Pietrogrande, M. C., Visentin, M., Scotto, F., Fuzzi, S., and Facchini, M. C.: Direct observation of aqueous secondary organic aerosol from biomass-burning emissions, Proc. Natl. Acad. Sci.

929   USA, 113, 10013−10018, https://doi.org/10.1073/pnas.1602212113, 2016.

930   Guo, H. Y., Xu, L., Bougiatioti, A., Cerully, K. M., Capps, S. L., Hite Jr., J.R., Carlton,

931   A. G., Lee, S. H., Bergin, M. H., Ng, N. L., Nenes, A., and Weber, R. J.:

932   Fine-particle water and pH in the southeastern United States, Atmos. Chem. Phys.,

933   15, 5211−5228, https://doi.org/10.5194/acp-15-5211-2015, 2015.

934   Gyawali, M., Arnott, W. P., Lewis, K., and Moosmüller, H.: In situ aerosol optics in

935   Reno, NV, USA during and after the summer 2008 California wildfires and the

936   influence of absorbing and non-absorbing organic coatings on spectral light

937   absorption, Atmos. Chem. Phys., 9, 8007−8015,

938   https://doi.org/10.5194/acp-9-8007-2009, 2009.

939   He, M., Wang, X. R., Han, L., Feng, X. D., and M, X.: Emission Inventory of Crop

940   Residues Field Burning and Its Temporal and Spatial Distribution in Sichuan

941   Province, Environ. Sci., 36, 1208−1216,

942   https://doi.org/10.13227/j.hjkx.2015.04.010, 2015.

943   Hennigan, C. J., Izumi, J., Sullivan, A. P., Weber, R. J., and Nenes, A.: A critical

944   evaluation of proxy methods used to estimate the acidity of atmospheric particles,

945   Atmos. Chem. Phys., 15, 2775–2790, https://doi.org/10.5194/acp-15-2775-2015,

946   2015.

947   Hennigan, C. J., Sullivan, A. P., Collett, J. L., and Robinson, A. L.: Levoglucosan

948   stability in biomass burning particles exposed to hydroxyl radicals, Geophys. Res.

949   Lett., 37, L09806, https://doi.org/10.1029/2010GL043088, 2010.

950   Herrmann, H., Schaefer, T., Tilgner, A., Styler, S. A., Weller, C., Teich, M., and Otto,

951   T.: Tropospheric Aqueous-Phase Chemistry: Kinetics, Mechanisms, and Its

952   Coupling to a Changing Gas Phase, Chem. Rev., 115, 4259−4334,

953   https://doi.org/10.1021/cr500447k, 2015.

954   Huang, R. J., Zhang, Y. L., Bozzetti, C., Ho, K. F., Cao, J. J., Han, Y. M., Daellenbach,

955   K. R., Slowik, J. G., Platt, S. M., Canonaco, F., Zotter, P., Wolf, R., Pieber, S. M.,

956   Bruns, E. A., Crippa, M., Ciarelli, G., Piazzalunga, A., Schwikowski, M.,

957   Abbaszade, G., Schnelle-Kreis, J., Zimmermann, R., An, Z. S., Szidat, S.,

958   Baltensperger, U., El Haddad, I., and Prevot, A. S.: High secondary aerosol

contribution to particulate pollution during haze events in China, Nature, 514, 218−222, https://doi.org/10.1038/nature13774, 2014.

Huang, R. J., He, Y., Duan, J., Li, Y. J., Chen, Q., Zheng, Y., Chen, Y., Hu, W. W., Lin, C. S., Ni, H. Y., Dai, W. T., Cao, J. J., Wu, Y. F., Zhang, R. J., Xu, W., Ovadnevaite, J., Ceburnis, D., Hoffmann, T., and O'Dowd, C. D.: Contrasting sources and processes of particulate species in haze days with low and high relative humidity in wintertime Beijing, Atmos. Chem. Phys., 20, 9101−9114, https://doi.org/10.5194/acp-20-9101-2020, 2020.

Huang, X. J., Liu, Z., Ge, Y. Z., Li, Q., Wang, X. F., Fu, H. B., Zhu, J., Zhou, B., Wang, L., George, C., Wang, Y., Wang, X. F., Su, J. X., Xue, L. K., Yu, S. C., Mellouki, A., and Chen, J. M.: Aerosol high water contents favor sulfate and secondary organic aerosol formation from fossil fuel combustion emissions, npj Clim. Atmos. Sci., 6, 173, https://doi.org/10.1038/s41612-023-00504-1, 2023.

Jimenez, J. L., Canagaratna, M. R., Donahue, N. M., Prevot, A. S. H., Zhang, Q., Kroll, J. H., DeCarlo, P. F., Allan, J. D., Coe, H., Ng, N. L., Aiken, A. C., Docherty, K. S., Ulbrich, I. M., Grieshop, A. P., Robinson, A. L., Duplissy, J., Smith, J. D., Wilson, K. R., Lanz, V. A., Hueglin, C., Sun, Y. L., Tian, J., Laaksonen, A., Raatikainen, T., Rautiainen, J., Vaattovaara, P., Ehn, M., Kulmala, M., Tomlinson, J. M., Collins, D. R., Cubison, M. J., Dunlea, J., Huffman, J. A., Onasch, T. B., Alfarra, M. R., Williams, P. I., Bower, K., Kondo, Y., Schneider, J., Drewnick, F., Borrmann, S., Weimer, S., Demerjian, K., Salcedo, D., Cottrell, L., Griffin, R., Takami, A., Miyoshi, T., Hatakeyama, S., Shimono, A., Sun, J. Y., Zhang, Y. M., Dzepina, K., Kimmel, J. R., Sueper, D., Jayne, J. T., Herndon, S. C., Trimborn, A. M., Williams, L. R., Wood, E. C., Middlebrook, A. M., Kolb, C. E., Baltensperger, U., and Worsnop, D. R.: Evolution of Organic Aerosols in the Atmosphere, Science, 326, 1525−1529, https://doi.org/10.1126/science.1180353, 2009.

Kampf, C. J., Jakob, R., and Hoffmann, T.: Identification and characterization of aging products in the glyoxal/ammonium sulfate system – implications for light-absorbing material in atmospheric aerosols, Atmos. Chem. Phys., 12, 6323−6333, https://doi.org/10.5194/acp-12-6323-2012, 2012.

Kim, H., Collier, S., Ge, X. L., Xu, J. Z., Sun, Y. L., Jiang, W. Q., Wang, Y. L., Herckes, P., and Zhang, Q.: Chemical processing of water-soluble species and formation of secondary organic aerosol in fogs, Atmos. Environ., 200, 158−166, https://doi.org/10.1016/j.atmosenv.2018.11.062, 2019.

Kirchstetter, T. W. and Novakov T.: Evidence that the spectral dependence of light absorption by aerosols is affected by organic carbon, J. Geophys. Res., 109, D21208, https://doi.org/10.1029/2004JD004999, 2004.

Kondo, Y., Komazaki, Y., Miyazaki, Y., Moteki, N., Takegawa, N., Kodama, D., Deguchi, S., Nogami, M., Fukuda, M., Miyakawa, T., Morino, Y., Koike, M., Sakurai, H., and Ehara, K.: Temporal Variations of Elemental Carbon in Tokyo, J. Geophys. Res., 111, D12205, https://doi.org/10.1029/2005JD006257, 2006.

Kourtchev, I., Giorio, C., Manninen, A., Wilson, E., Mahon, B., Aalto, J., Kajos, M., Venables, D., Ruuskanen, T., Levula, J., Loponen, M., Connors, S., Harris, N., Zhao, D. F., Kiendler-Scharr, A., Mentel, T., Rudich, Y., Hallquist, M., Doussin, J. F., Maenhaut, W., Bäck, J., Petäjä, T., Wenger, J., Kulmala, Ma., and Kalberer, M.: Enhanced Volatile Organic Compounds emissions and organic aerosol mass increase the oligomer content of atmospheric aerosols, Sci. Rep., 6, 35038, https://doi.org/10.1038/srep35038, 2016.

Kroflic, A., Grilc, M., and Grgic, I.: Unraveling pathways of guaiacol nitration in atmospheric waters: nitrite, a source of reactive nitronium ion in the atmosphere, Environ. Sci. Technol., 49, 9150−9158, https://doi.org/10.1021/acs.est.5b01811, 2015.

Lack, D. A., and Langridge, J. M.: On the attribution of black and brown carbon light absorption using the Ångström exponent, Atmos. Chem. Phys., 13, 10535−10543, https://doi.org/10.5194/acp-13-10535-2013, 2013.

Lanz, V. A., Alfarra, M. R., Baltensperger, U., Buchmann, B., Hueglin, C., and Prévôt, A. S. H.: Source apportionment of submicron organic aerosols at an urban site by factor analytical modelling of aerosol mass spectra, Atmos. Chem. Phys., 7, 1503−1522, doi:10.5194/acp-7-1503-2007, 2007.

Laskin, A., Laskin, J., and Nizkorodov, S. A.: Chemistry of atmospheric brown carbon,

Chem. Rev., 115, 4335−4382, https://doi.org/10.1021/cr5006167, 2015.

Lee, A. K., Zhao, R., Li, R., Liggio, J., Li, S. M., and Abbatt, J. P.: Formation of Light Absorbing Organo-Nitrogen Species from Evaporation of Droplets Containing Glyoxal and Ammonium Sulfate, Environ. Sci. Technol., 47, 12819−12826, https://doi.org/10.1021/es402687w, 2013.

Lei, Y., Lei, X., Tian, G., Yang, J., Huang, D., Yang, X., Chen, C. C., and Zhao, J. C.: Optical Variation and Molecular Transformation of Brown Carbon During Oxidation by $NO_3\bullet$ in the Aqueous Phase, Environ. Sci. Technol., 58, 3353−3362, https://doi.org/10.1021/acs.est.3c08726, 2024.

Li, C. L., He, Q. F., Fang, Z., Brown, S. S., Laskin, A., Cohen, S. R., and Rudich, Y.: Laboratory Insights into the Diel Cycle of Optical and Chemical Transformations of Biomass Burning Brown Carbon Aerosols, Environ. Sci. Technol., 54, 11827−11837, https://dx.doi.org/10.1021/acs.est.0c04310, 2020.

Li, F. H., Zhou, S. Z., Du, L., Zhao, J., Hang, J., and Wang, X. M.: Aqueous-phase chemistry of atmospheric phenolic compounds: A critical review of laboratory studies, Sci. Total Environ., 856, 158895, https://doi.org/10.1016/j.scitotenv.2022.158895, 2023.

Li, G., Bei, N., Tie, X., and Molina, L. T.: Aerosol effects on the photochemistry in Mexico City during MCMA-2006/MILAGRO campaign, Atmos. Chem. Phys., 11, 5169−5182, https://doi.org/10.5194/acp-11-5169-2011, 2011.

Li, Z. J., Tan, H. B., Zheng, J., Liu, L., Qin, Y. M., Wang, N., Li, F., Li ,Y. J., Cai, M. F., Ma, Y., and Chan, C. K.: Light absorption properties and potential sources of particulate brown carbon in the Pearl River Delta region of China, Atmos. Chem. Phys., 19, 11669−11685, https://doi.org/10.5194/acp-19-11669-2019, 2019.

Lim, Y. B., Tan, Y., Perri, M. J., Seitzinger, S. P., and Turpin, B. J.: Aqueous chemistry and its role in secondary organic aerosol (SOA) formation, Atmos. Chem. Phys., 10, 10521−10539, https://doi.org/10.5194/acp-10-10521-2010, 2010.

Liu, M. X., Song, Y., Zhou, T., Xu, Z. Y., Yan, C. Q., Zheng, M., Wu, Z. J., Hu, M., Wu, Y. S., and Zhu, T.: Fine particle pH during severe haze episodes in northern China, Geophys. Res. Lett., 44, 5213−5221, https://doi.org/10.1002/2017gl073210,

1049   2017.

1050   Liu, Y., Huang, R. J., Lin, C. S., Yuan, W., Li, Y. J., Zhong, H. B., Yang, L., Wang, T.,

1051   Huang, W., Xu, W., Huang, D. D., and Huang, C.: Nitrate-Photolysis Shortens the

1052   Lifetimes of Brown Carbon Tracers from Biomass Burning, Environ. Sci. Technol.,

1053   59, 640−649, https://doi.org/10.1021/acs.est.4c06123, 2024.

1054   Lorenzo, R. A. D., Washenfelder, R. A., Attwood, A. R., Guo, H., Xu, L., Ng, N. L.,

1055   Weber, R. J., Baumann, K., Edgerton, E., and Young, C. J.:

1056   Molecular-Size-Separated Brown Carbon Absorption for Biomass-Burning Aerosol

1057   at Multiple Field Sites, Environ. Sci. Technol., 51, 3128−3137,

1058   https://doi.org/10.1021/acs.est.6b06160, 2017.

1059   Lu, Z., Streets, D. G., Winijkul, E., Yan, F., Chen, Y., Bond, T. C., Feng, Y., Dubey, M.

1060   K., Liu, S., Pinto, J. P., and Carmichael, G. R.: Light absorption properties and

1061   radiative effects of primary organic aerosol emissions, Environ. Sci. Technol., 49,

1062   4868−4877, https://doi.org/10.1021/acs.est.5b00211, 2015.

1063   Luo, J. Q., Zhang, J. K., Huang, X. J ., Liu, Q., Luo, B., Zhang, W., Rao, Z. H., and

1064   Yu, Y. C.: Characteristics, evolution, and regional differences of biomass burning

1065   particles in the Sichuan Basin, China, J. Environ. Sci., 89, 35−46,

1066   https://doi.org/10.1016/j.jes.2019.09.015, 2020.

1067   Matthew, B. M., Middlebrook, A. M., and Onasch, T. B.: Collection Efficiencies in an

1068   Aerodyne Aerosol Mass Spectrometer as a Function of Particle Phase for

1069   Laboratory Generated Aerosols, Aerosol Sci. Technol., 42, 884−898,

1070   https://doi.org/10.1080/02786820802356797, 2008.

1071   McNeill, V. F.: Aqueous Organic Chemistry in the Atmosphere: Sources and Chemical

1072   Processing of Organic Aerosols, Environ. Sci. Technol., 49, 1237−1244,

1073   https://doi.org/10.1021/es5043707, 2015.

1074   Meng, J. J., Liu, X. D., Hou, Z. F., Yi, Y. A., Yan, L., Li, Z., Cao, J. J., Li, J. J., and

1075   Wang, G. H.: Molecular characteristics and stable carbon isotope compositions of

1076   dicarboxylic acids and related compounds in the urban atmosphere of the North

1077   China Plain: Implications for aqueous phase formation of SOA during the haze

1078   periods, Sci. Total Environ., 705, 135256,

1079   https://doi.org/10.1016/j.scitotenv.2019.135256, 2020.

1080   Middlebrook, A. M., Bahreini, R., Jimenez, J. L., and Canagaratna, M. R.: Evaluation

1081   of Composition-Dependent Collection Efficiencies for the Aerodyne Aerosol Mass

1082   Spectrometer using Field Data, Aerosol Sci. Technol., 46, 258−271,

1083   https://doi.org/10.1080/02786826.2011.620041, 2012.

1084   Ministry of Environmental Protection (MEP): P.R. Of China, China National Ambient

1085   Air   Quality   Standard   (GB   3095-2012),   http://kjs.mep.

1086   gov.cn/hjbhbz/bzwb/dqhjbh/dqhjzlbz/201203/t20120302_224165.htm, 2012.

1087   Moosmüller, H., Chakrabarty, R. K., and Arnott, W. P.: Aerosol light absorption and

1088   its   measurement: A   review,   J.   Quant.   Spectrosc.   Ra.,   110,   844−878,

1089   https://doi.org/10.1016/j.jqsrt.2009.02.035, 2009.

1090   Ng, N. L., Canagaratna, M. R., Jimenez, J. L., Chhabra, P. S., Seinfeld, J. H., and

1091   Worsnop, D. R.: Changes in organic aerosol composition with aging inferred from

1092   aerosol   mass   spectra,   Atmos.   Chem.   Phys.,   11,   6465−6474,

1093   https://doi.org/10.5194/acp-11-6465-2011, 2011a.

1094   Ng, N. L., Canagaratna, M. R., Jimenez, J. L., Zhang, Q., Ulbrich, I. M., and Worsnop,

1095   D.   R.:   Real-Time   Methods   for   Estimating   Organic   Component   Mass

1096   Concentrations from Aerosol Mass Spectrometer Data, Environ. Sci. Technol., 45,

1097   910−916, https://doi.org/10.1021/es102951k, 2011b.

1098   Ng, N. L., Canagaratna, M. R., Zhang, Q., Jimenez, J. L., Tian, J., Ulbrich, I. M.,

1099   Kroll, J. H., Docherty, K. S., Chhabra, P. S., Bahreini, R., Murphy, S. M., Seinfeld,

1100   J. H., Hildebrandt, L., Donahue, N. M., DeCarlo, P. F., Lanz, V. A., Prévôt, A. S. H.,

1101   Dinar, E., Rudich, Y., and Worsnop, D. R.: Organic aerosol components observed

1102   in Northern Hemispheric datasets from Aerosol Mass Spectrometry, Atmos. Chem.

1103   Phys., 10, 4625−4641, https://doi.org/10.5194/acp-10-4625-2010, 2010.

1104   Ng, N. L., Herndon, S. C., Trimborn, A., Canagaratna, M. R., Croteau, P. L., Onasch,

1105   T. B., Sueper, D., Worsnop, D. R., Zhang, Q., Sun, Y. L., and Jayne J. T.: An

1106   Aerosol Chemical Speciation Monitor (ACSM) for Routine Monitoring of the

1107   Composition and Mass Concentrations of Ambient Aerosol, Aerosol Sci. Technol.,

1108   45, 780−794, https://doi.org/10.1080/02786826.2011.560211, 2011c.

1109   Nguyen, T. K. V., Zhang, Q., Jimenez, J. L., Pike, M., and Carlton, A. G.: Liquid

1110   Water: Ubiquitous Contributor to Aerosol Mass, Environ. Sci. Technol. Lett., 3,

1111   257−263, https://doi.org/10.1021/acs.estlett.6b00167, 2016.

1112   Nozière, B., and Esteve, W.: Light-absorbing aldol condensation products in acidic

1113   aerosols: Spectra, kinetics, and contribution to the absorption index, Atmos.

1114   Environ., 41, 1150−1163, https://doi.org/10.1016/j.atmosenv.2006.10.001, 2007.

1115   Nozière, B., Dziedzic, P., and Córdova, A.: Products and Kinetics of the Liquid-Phase

1116   Reaction of Glyoxal Catalyzed by Ammonium Ions (NH_4^+), J. Phys. Chem. A, 113,

1117   231−237, https://doi.org/10.1021/jp8078293, 2009.

1118   Ortega, A. M., Ortega, D. A., Cubison, M. J., Brune, W. H., Bon, D., Gouw de, J. A.,

1119   and Jimenez, J. L.: Secondary organic aerosol formation and primary organic

1120   aerosol oxidation from biomass-burning smoke in a flow reactor during FLAME-3,

1121   Atmos.   Chem.   Phys.,   13,   11551−11571,

1122   https://doi.org/10.5194/acp-13-11551-2013, 2013.

1123   Ortiz-Montalvo, D. L., Lim, Y. B., Perri, M. J., Seitzinger, S. P., and Turpin, B. J.:

1124   Volatility and Yield of Glycolaldehyde SOA Formed through Aqueous

1125   Photochemistry and Droplet Evaporation, Aerosol Sci. Technol., 46, 1002−1014,

1126   https://doi.org/10.1080/02786826.2012.686676, 2012.

1127   Paatero, P.: The Multilinear Engine: A Table-Driven, Least Squares Program for

1128   Solving Multilinear Problems, Including the n-Way Parallel Factor Analysis Model,

1129   J.   Comput.   Graph.   Stat.,   8,   854−888,

1130   https://doi.org/10.1080/10618600.1999.10474853, 1999.

1131   Paatero, P. and Hopke, P. K.: Discarding or downweighting high-noise variables in

1132   factor   analytic   models,   Anal.   Chim.   Acta.,   490,   277−289,

1133   https://doi.org/10.1016/S0003-2670(02)01643-4, 2003.

1134   Paatero, P. and Tapper, U.: Positive matrix factorization: A non-negative factor model

1135   with optimal utilization of error estimates of data values, Environmetrics, 5,

1136   111−126, https://doi.org/10.1002/env.3170050203, 1994.

1137   Paglione, M., Gilardoni, S., Rinaldi, M., Decesari, S., Zanca, N., Sandrini, S.,

1138   Giulianelli, L., Bacco, D., Ferrari, S., Poluzzi, V., Scotto, F., Trentini, A., Poulain,

L., Herrmann, H., Wiedensohler, A., Canonaco, F., Prévôt, A. S. H., Massoli, P., Carbone, C., Facchini, M. C., and Fuzzi, S. C.: The impact of biomass burning and aqueous-phase processing on air quality: a multi-year source apportionment study in the Po Valley, Italy, Atmos. Chem. Phys., 20, 1233−1254, https://doi.org/10.5194/acp-20-1233-2020, 2020.

Pang, H. W., Zhang, Q., Lu, X. H., Li, K. N., Chen, H., Chen, J. M., Yang, X., Ma, Y. G., Ma, J. L., and Huang, C.: Nitrite-Mediated Photooxidation of Vanillin in the Atmospheric Aqueous Phase, Environ. Sci. Technol., 53, 14253−14263, https://doi.org/10.1021/acs.est.9b03649, 2019.

Peng, C., Tian, M., Chen, Y., Wang, H. B., Zhang, L. M., Shi, G. M., Liu, Y., Yang, F. M., and Zhai, C. Z.: Characteristics, Formation Mechanisms and Potential Transport Pathways of $PM_{2.5}$ at a Rural Background Site in Chongqing, Southwest China, Aerosol Air Qual. Res., 19, 1980−1992, https://doi.org/10.4209/aaqr.2019.01.0010, 2019.

Peng, C., Tian, M., Shi, G. M., Zhang, S. M., Long, X., Che, H. X., Zhong, J., You, X. Y., Bao, Z. E., Yang, F. M., Qi, X., Zhai, C. Z., and Chen, Y.: Sources and light absorption of brown carbon in urban areas of the Sichuan Basin, China: Contribution from biomass burning and secondary formation, Atmos. Res., 318, 107992, https://doi.org/10.1016/j.atmosres.2025.107992, 2025.

Powelson, M. H., Espelien, B. M., Hawkins, L. N., Galloway, M. M., and Haan, D. O. D.: Brown Carbon Formation by Aqueous-Phase Carbonyl Compound Reactions with Amines and Ammonium Sulfate, Environ. Sci. Technol., 48, 985−993, https://doi.org/10.1021/es4038325, 2014.

Qin, Y. M., Tan, H. B., Li, Y. J., Li, Z. J., Schurman, M. I., Liu, L., Wu, C., and Chan, C. K.: Chemical characteristics of brown carbon in atmospheric particles at a suburban site near Guangzhou, China, Atmos. Chem. Phys., 18, 16409−16418, https://doi.org/10.5194/acp-18-16409-2018, 2018.

Qiu, X., Duan, L., Chai, F., Wang, S., Yu, Q., and Wang, S.: Deriving High-Resolution Emission Inventory of Open Biomass Burning in China based on Satellite Observations, Environ. Sci. Technol., 50, 11779−11786,

https://doi.org/10.1021/acs.est.6b02705, 2016.

Saleh, R., Hennigan, C. J., McMeeking, G. R., Chuang, W. K., Robinson, E. S., Coe, H., Donahue, N. M., and Robinson, A. L.: Absorptivity of brown carbon in fresh and photo-chemically aged biomass-burning emissions, Atmos. Chem. Phys., 13, 7683−7693, https://doi.org/10.5194/acp-13-7683-2013, 2013.

Saleh, R., Robinson, E. S., Tkacik, D. S., Ahern, A. T., Liu, S., Aiken, A. C., Sullivan, R. C., Presto, A. A., Dubey, M. K., Yokelson, R. J., Donahue, N. M., and Robinson, A. L.: Brownness of organics in aerosols from biomass burning linked to their black carbon content, Nat. Geosci., 7, 647−650, https://doi.org/10.1038/ngeo2220, 2014.

Sareen, N., Moussa, S. G., and McNeill, V. F.: Photochemical Aging of Light-Absorbing Secondary Organic Aerosol Material, J. Phys. Chem. A, 117, 2987−2996, https://doi.org/10.1021/jp309413j, 2013.

Shrivastava, M., Cappa, C. D., Fan, J. W., Goldstein, A. H., Guenther, A. B., Jimenez, J. L., Kuang, C. A., Laskin, A., Martin, S. T., Ng, N. L., Petaja, T., Pierce, J. R., Rasch, P. J., Roldin, P., Seinfeld, J. H., Shilling, J., Smith, J. N., Thornton, J. A., Volkamer, R., Wang, J., Worsnop, D. R., Zaveri, R. A., Zelenyuk, A., and Zhang, Q.: Recent advances in understanding secondary organic aerosol: Implications for global climate forcing, Rev. Geophys., 55, 509−559, doi:10.1002/2016RG000540, 2017.

Sun, Y. L., Du, W., Fu, P. Q., Wang, Q. Q., Li, J., Ge, X. L., Zhang, Q., Zhu, C. M., Ren, L. J., Xu, W. Q., Zhao, J., Han, T. T., Worsnop, D. R., and Wang, Z. F.: Primary and secondary aerosols in Beijing in winter: sources, variations and processes, Atmos. Chem. Phys., 16, 8309−8329, https://doi.org/10.5194/acp-16-8309-2016, 2016a.

Sun, Y. L., Jiang, Q., Xu, Y. S., Ma, Y., Zhang, Y. J., Liu, X. G., Li, W. J., Wang, F., Li, J., Wang, P. C., and Li, Z. Q.: Aerosol characterization over the North China Plain: Haze life cycle and biomass burning impacts in summer, J. Geophys. Res.: Atmos., 121, 2508−2521, https://doi.org/10.1002/ 2015jd024261, 2016b.

Sun, Y. L., Zhang, Q., Anastasio, C., and Sun, J.: Insights into secondary organic

aerosol formed via aqueous-phase reactions of phenolic compounds based on high resolution mass spectrometry, Atmos. Chem. Phys., 10, 4809−4822, https://doi.org/10.5194/acp-10-4809-2010, 2010.

Tan, Y., Lim, Y. B., Altieri, K. E., Seitzinger, S. P., and Turpin, B. J.: Mechanisms leading to oligomers and SOA through aqueous photooxidation: insights from OH radical oxidation of acetic acid and methylglyoxal, Atmos. Chem. Phys., 12, 801−813, https://doi.org/10.5194/acp-12-801-2012, 2012.

Tang, H. H., Li, Z. L., Tian, M., Peng, C., Ding, Y., Chen, M. L., Wang, X., C., Chen, Y., Yang, F. M., and Zhai, C. Z.: Formation of Oxidized Organic Aerosols in Winter Haze in a Megacity of Southwest China: Implication for the Importance of Biomass Burning, J. Geophys. Res. Atmos., 130, e2025JD044028, https://doi.org/10.1029/2025JD044028, 2025.

Tao, J., Gao, J., Zhang, L., Zhang, R., Che, H., Zhang, Z., Lin, Z., Jing, J., Cao, J., and Hsu, S. C.: $PM_{2.5}$ pollution in a megacity of southwest China: source apportionment and implication, Atmos. Chem. Phys., c14, 8679−8699, https://doi.org/10.5194/acp-14-8679-2014, 2014.

Tian M., Liu Y., Yang F. M., Zhang L. M., Peng C., Chen Y., Shi G. M., Wang H. B., Luo B., Jiang C. T., Li B., Takeda N., and Koizumi K.: Increasing importance of nitrate formation for heavy aerosol pollution in two megacities in Sichuan Basin, southwest China, Environ. Pollut., 250, 898−905, https://doi.org/10.1016/j.envpol.2019.04.098, 2019.

Wang, G. H., Zhang, R. Y., Gomez, M. E., Yang, L. X., Zamora, M. L., Hu, M., Lin, Y., Peng, J. F., Guo, S., Meng, J. J., Li, J. J., Cheng, C. L., Hu T. F., Ren, Y. Q., Wang, Y. S., Gao, J., Cao, J. J., An, Z. S., Zhou, W. J., Li, G. H., Wang, J. Y., Tian, P. F., Marrero-Ortiz, W., Secrest, J., Du, Z. F., Zheng, J., Shang, D. J., Zeng, L. M., Shao, M., Wang, W. G., Huang, Y., Wang, Y., Zhu, Y. J., Li, Y. X., Hu, J. X., Pan, B., Cai, L., Cheng, Y. T., Ji, Y. M., Zhang, F., Rosenfeld, D., Liss, P. S., Duce, R. A., Kolb, C. E., and Molina, M. J.: Persistent sulfate formation from London Fog to Chinese haze, Proc. Natl. Acad. Sci. USA, 113, 13630−13635, https://doi.org/10.1073/pnas.1616540113, 2016.

Wang, H. B., Tian, M., Chen, Y., Shi, G. M., Liu, Y., Yang, F. M., Zhang, L. M., Deng, L. Q., Yu, J. Y., Peng, C., and Cao, X. Y.: Seasonal characteristics, formation mechanisms and source origins of PM$_{2.5}$ in two megacities in Sichuan Basin, China, Atmos. Chem. Phys., 18, 865−881, https://doi.org/10.5194/acp-18-865-2018, 2018.

Wang, H. B., Zhang, L. M., Huo, T. T., Wang, B., Yang, F. M., Chen, Y., Tian, M., Qiao, B. Q., and Peng, C.: Application of parallel factor analysis model to decompose excitation-emission matrix fluorescence spectra for characterizing sources of water-soluble brown carbon in PM$_{2.5}$, Atmos. Environ., 223, 117192, https://doi.org/10.1016/j.atmosenv.2019.117192, 2019a.

Wang, J. F., Ye, J. H., Zhang, Q., Zhao, J., Wu, Y. Z., Li, J. Y., Liu, D. T., Li, W. J., Zhang, Y. G., Wu, C., Xie, C. H., Qin, Y. M., Lei, Y. L., Huang, X. P., Guo, J. P., Liu, P. F., Fu, P. Q., Li, Y. J., Lee, H. C., Choi, H., Zhang, J., Liao, H., Chen, M. D., Sun, Y. L., Ge, X. L., Martin, S. T., and Jacob, D. J.: Aqueous production of secondary organic aerosol from fossil-fuel emissions in winter Beijing haze, Proc. Natl. Acad. Sci. USA, 118, e2022179118, https://doi.org/10.1073/pnas.2022179118, 2021.

Wang, Q. Y., Ye, J. H., Wang, Y. C., Zhang, T., Ran, W. K., Wu, Y. F., Tian, J., Li, L., Zhou, Y. Q., Ho, H. S. S., Dang, B., Zhang, Q., Zhang, R. J., Chen, Y., Zhu, C. S., and Cao, J. J.: Wintertime Optical Properties of Primary and Secondary Brown Carbon at a Regional Site in the North China Plain, Environ. Sci. Technol., 53, 12389−12397, https://doi.org/10.1021/acs.est.9b03406, 2019b.

Washenfelder, R. A., Attwood, A. R., Brock, C. A., Guo, H., Xu, L., Weber, R. J., Ng, N. L., Allen, H. M., Ayres, B. R., Baumann, K., Cohen, R. C., Draper, D. C., Duffey, K. C., Edgerton, E., Fry, J. L., Hu, W. W., Jimenez, J. L., Palm, B. B., Romer, P., Stone, E. A., Wooldridge, P. J., and Brown, S. S.: Biomass burning dominates brown carbon absorption in the rural southeastern United States, Geophys. Res. Lett., 42, 653−664, https://doi.org/10.1002/2014gl062444, 2015.

Wu, C. and Yu, J. Z.: Determination of primary combustion source organic carbon-to-elemental carbon (OC/EC) ratio using ambient OC and EC measurements: Secondary OC-EC correlation minimization method, Atmos. Chem.

Phys., 16, 5453−5465, https://doi.org/10.5194/acp-16-5453-2016, 2016.

Wu, H., Peng, C., Zhai, T. Y., Deng, J. C., Lu, P. L., Li, Z. L., Chen, Y., Tian, M., Bao, Z. E., Long, X., Yang, F. M., and Zhai, C. Z.: Characteristics of light absorption and environmental effects of Brown carbon aerosol in Chongqing during summer and winter based on online measurement: Implications of secondary formation, Atmos. Environ., 338, 120843, https://doi.org/10.1016/j.atmosenv.2024.120843, 2024.

Xie, C. H., Xu, W. Q., Wang, J. F., Wang, Q. Q., Liu, D. T., Tang, G. Q., Chen, P., Du, W., Zhao, J., Zhang, Y. J., Zhou, W., Han, T. T., Bian, Q. Y., Li, J., Fu, P. Q., Wang, Z. F., Ge, X. L., Allan, J., Coe, H., and Sun, Y. L.: Vertical characterization of aerosol optical properties and brown carbon in winter in urban Beijing, China, Atmos. Chem. Phys., 19, 165−179, https://doi.org/10.5194/acp-19-165-2019, 2019.

Xu, B. Q., Zhang, G., Gustafsson, Ö., Kawamura, K., Li, J., Andersson, A., Bikkina, S., Kunwar, B., Pokhrel, A., Zhong, G. C., Zhao, S. Z., Li, J., Huang, C., Cheng, Z. N., Zhu, S. Y., Peng, P. A., and Sheng, G. Y.: Large contribution of fossil-derived components to aqueous secondary organic aerosols in China, Nat. Commun., 13, 5115, https://doi.org/10.1038/s41467-022-32863-3, 2022.

Xu, W. Q., Han, T. T., Du, W., Wang, Q. Q., Chen, C., Zhao, J., Zhang, Y. J., Li, J., Fu, P. Q., Wang, Z. F., Worsnop, D. R., and Sun, Y. L.: Effects of Aqueous-Phase and Photochemical Processing on Secondary Organic Aerosol Formation and Evolution in Beijing, China, Environ. Sci. Technol., 51, 762−770, https://doi.org/10.1021/acs.est.6b04498, 2017.

Xu, W. Q., Sun, Y. L., Chen, C., Du, W., Han, T. T., Wang, Q. Q., Fu, P. Q., Wang, Z. F., Zhao, X. J., Zhou, L. B., Ji, D. S., Wang, P. C., and Worsnop, D. R.: Aerosol composition, oxidation properties, and sources in Beijing: results from the 2014 Asia-Pacific Economic Cooperation summit study, Atmos. Chem. Phys., 15, 13681−13698, https://doi.org/10.5194/acp-15-13681-2015, 2015.

Xu, W. Q., Sun, Y. L., Wang, Q. Q., Zhao, J., Wang, J. F., Ge, X. L., Xie, C. J., Zhou, W., Du, W., Li, J., Fu, P. Q., Wang, Z. F., Worsnop, D. R., and Coe, H.: Changes in Aerosol Chemistry From 2014 to 2016 in Winter in Beijing: Insights From

High-Resolution Aerosol Mass Spectrometry, J. Geophys. Res.: Atmos., 124, 1132−1147, https://doi.org/10.1029/2018JD029245, 2019.

Yan, C. Q., Zheng, M., Bosch, C., Andersson, A., Desyaterik, Y., Sullivan, A. P., Collett, J. L., Zhao, B., Wang, S. X., He, K. B., and Gustafsson, Ö.: Important fossil source contribution to brown carbon in Beijing during winter, Sci. Rep., 7, 43182, https://doi.org/10.1038/srep43182, 2017.

Yang, F. M., Tan, J., Zhao, Q., Du, Z., He, K. B., Ma, Y. L., Duan, F. K., Chen, G., and Zhao, Q.: Characteristics of $PM_{2.5}$ speciation in representative megacities and across China, Atmos. Chem. Phys., 11, 5207−5219, https://doi.org/10.5194/acp-11-5207-2011, 2011.

Yang, J. W., Au, W. C., Law, H., Lam, C. H., and Nah, T.: Formation and evolution of brown carbon during aqueous-phase nitrate-mediated photooxidation of guaiacol and 5-nitroguaiacol, Atmos. Environ., 254, 118401, https://doi.org/10.1016/j.atmosenv.2021.118401, 2021.

Yang, W., Xie, S., Zhang, Z., Hu, J., Zhang, L., Lei, X., Zhong, L., Hao, Y., and Shi, F.: Characteristics and sources of carbonaceous aerosol across urban and rural sites in a rapidly urbanized but low-level industrialized city in the Sichuan Basin, China, Environ. Sci. Pollut. R., 26, 26646−26663, https://doi.org/10.1007/s11356-019-05242-7, 2019.

Ye, Z. L., Qu, Z. X., Ma, S. S., Luo, S. P., Chen, Y. T., Chen, H., Chen, Y. F., Zhao, Z. Z., Chen, M. D., and Ge, X. L.: A comprehensive investigation of aqueous-phase photochemical oxidation of 4-ethylphenol, Sci. Total Environ., 685, 976−985, https://doi.org/10.1016/j.scitotenv.2019.06.276, 2019.

Yokelson, R. J., Urbanski, S. P., Atlas, E. L., Toohey, D. W., Alvarado, E. C., Crounse, J. D., Wennberg, P. O., Fisher, M. E., Wold, C. E., Campos, T. L., Adachi, K., Buseck, P. R., and Hao, W. M.: Emissions from forest fires near Mexico City, Atmos. Chem. Phys., 7, 5569−5584, https://doi.org/10.5194/acp-7-5569-2007, 2007.

Yu, L., Smith, J., Laskin, A., Anastasio, C., Laskin, J., Zhang, Q.: Chemical characterization of SOA formed from aqueous-phase reactions of phenols with the

triplet excited state of carbonyl and hydroxyl radical, Atmos. Chem. Phys., 14, 13801−13816, https://doi.org/10.5194/acp-14-13801-2014, 2014.

Yu, L., Smith, J., Laskin, A., George, K. M., Anastasio, C., Laskin, J., Dillner, A. M., and Zhang, Q.: Molecular transformations of phenolic SOA during photochemical aging in the aqueous phase: competition among oligomerization, functionalization, and fragmentation, Atmos. Chem. Phys., 16, 4511−4527, https://doi.org/10.5194/acp-16-4511-2016, 2016.

Zeng, X., Bao, Z., Zhou, J., Shi, G., Zhou, L., Zhang, S., Qi, X., Lu, K., Zhai, C., Li, Z., Li, X., Peng, C., Yang, F., Tang, M., Feng, M., Tan, Q., and Chen, Y.: Effects of photochemical and aqueous-phase oxidation on secondary formation during the 31st FISU Summer World University Games, 2023, J. Environ. Sci., 162, 810−820, https://doi.org/10.1016/j.jes.2025.08.039, 2025.

Zhang, X. Y., Bao, Z. R., Zhang, L. Y., Zhou, J. W., Che, H. X., Li, Q., Tian, M., Yang, F. M., and Chen, Y.: Biomass burning and aqueous reactions drive the elevation of wintertime $PM_{2.5}$ in the rural area of the Sichuan basin, China, Atmos. Environ., 306, 119779, https://doi.org/10.1016/j.atmosenv.2023.119779, 2023.

Zhang, X. Y., Liu, H. X., Cheng, J. L., Song, W., Wang, H. C., Zhang, Y. L., and Wang, X. M.: Gas-Phase Oxidation of Guaiacol by NO_3 Radicals: Kinetic Measurements and Implications, ACS ES&T Air, 2, 903−910, https://doi.org/10.1021/acsestair.4c00353, 2025.

Zhao, J., Du, W., Zhang, Y. J., Wang, Q. Q., Chen, C., Xu, W. Q., Han, T. T., Wang, Y. Y., Fu, P. Q., Wang, Z. F., Li, Z. Q., and Sun, Y. L.: Insights into aerosol chemistry during the 2015 China Victory Day parade: results from simultaneous measurements at ground level and 260 m in Beijing, Atmos. Chem. Phys., 17, 3215−3232, https://doi.org/10.5194/acp-17-3215-2017, 2017.

Zhao, J., Qiu, Y. M.,Zhou, W., Xu, W. Q., Wang, J. F., Zhang, Y. J., Li, L. J., Xie, C. H., Wang, Q. Q., Du, W., Worsnop, D. R., Canagaratna, M. R., Zhou, L. B., Ge, X. L., Fu, P. Q., Li, J., Wang, Z. F., Donahue, N. M., and Sun, Y. L.: Organic Aerosol Processing During Winter Severe Haze Episodes in Beijing, J. Geophys. Res.: Atmos., 124, 10248−10263, https://doi.org/10.1029/2019JD030832, 2019.

Zhao, R., Lee, A. K. Y., Huang, L., Li, X., Yang, F., and Abbatt, J. P. D.: Photochemical processing of aqueous atmospheric brown carbon, Atmos. Chem. Phys., 15, 6087−6100, https://doi.org/10.5194/acp-15-6087-2015, 2015.

Zhao, R., Mungall, E. L., Lee, A. K. Y., Aljawhary, D., and Abbatt, J. P. D.: Aqueous-phase photooxidation of levoglucosan – a mechanistic study using aerosol time-of-flight chemical ionization mass spectrometry (Aerosol ToF-CIMS), Atmos. Chem. Phys., 14, 9695−9706, https://doi.org/10.5194/acp-14-9695-2014, 2014.

Zhong, H. B., Huang, R. J., Chang, Y. H., Duan, J., Lin, C. S., and Chen, Y.: Enhanced formation of secondary organic aerosol from photochemical oxidation during the COVID-19 lockdown in a background site in Northwest China, Sci. Total Environ., 778, 144947, https://doi.org/10.1016/j.scitotenv.2021.144947, 2021.

Zhu, C. S., Cao, J. J., Hu, T. F., Shen, Z. X., Tie, X. X., Huang, H., Wang, Q. Y., Huang, R. J., Zhao, Z. Z., Mocnik, G., and Hansen, A. D. A.: Spectral dependence of aerosol light absorption at an urban and a remote site over the Tibetan Plateau, Sci. Total Environ., 590−591, 14−21, https://doi.org/10.1016/j.scitotenv.2017.03.057, 2017.

Zhu, L. W., Cui, Y. J., Ge, X. L., Ye, Z. l., and Zhao, Z. Z.: Aqueous-phase photochemical oxidation of extracted WSOC in $PM_{2.5}$ from biomass burning, China Environ. Sci., 43, 1014−1025, https://doi.org/10.19674/j.cnki.issn1000-6923.20220928.004, 2023.